Recommended mineral-melt partition coefficients for FRTEs (Cu), Ga and Ge during mantle melting

Véronique Le Roux[1], Rajdeep Dasgupta [2] and Cin-Ty A. Lee [2]

[1] Woods Hole Oceanographic Institution, MS#08, 266 Woods Hole Road, Woods Hole MA 02543 U.S.A.

[2] Department of Earth Science, Rice University, MS-126, 6100 Main Street, Houston TX 77005 U.S.A.

ABSTRACT

First-row transition element (FRTE) concentrations in primitive mantle-derived melts have been used as direct indicators of mantle source mineralogy (e.g., Ti, Mn, Fe, Co, Ni, Zn) and as proxies to trace the oxidation state of the mantle (e.g., Sc, V Cu, Zn). Ga and Ge, which share chemical similarities with FRTEs, may also have the ability to trace mineralogical heterogeneities in the source of mantle-derived melts. Although the partitioning behaviors of most FRTEs are well constrained during mantle melting, partition coefficients of Cu, Ga, and Ge between mantle minerals and melt are still uncertain. Here we report new measurements that constrain partition coefficients of Cu, Ga, and Ge between olivine (Ol), orthopyroxene (Opx), clinopyroxene (Cpx), and basaltic melt from graphite capsule experiments carried out at 1.5-2 GPa and 1290-1500 °C. We suggest that discrepancies between recent experimental studies on Cu partitioning reflect one or more of the following causes: compositional control on partitioning, the effect of oxygen fugacity, Cu loss, Fe loss, non-henrian behavior, and/or lack of complete chemical equilibrium. The partitioning values obtained from this study are 0.13 (±

0.06), 0.12 (±3), and 0.09 for $D_{Cu}^{Ol/melt}$, $D_{Cu}^{Opx/melt}$, and $D_{Cu}^{Cpx/melt}$, respectively. Using values from this study and from the literature, we show that melting of a sulfide-bearing peridotite source with an initial $D_{Cu}^{peridotite/melt}$ ranging from 0.49 to 0.60 can explain the Cu content of primitive MORBs. Here, we also support the hypothesis that Ga partitioning between pyroxenes and melt strongly depends on the Al_2O_3 content of pyroxenes. Using pyroxene compositions from experiments, and previous partition data from literature, we recommend $D_{Ga}^{Px/melt}$ values for low-*P* (1.5 GPa) spinel peridotite melting ($D_{Ga}^{Opx/melt}$ = 0.23 and $D_{Ga}^{Cpx/melt}$ = 0.28), intermediate-*P* (2.8 GPa) spinel peridotite melting ($D_{Ga}^{Opx/melt}$ = 0.42 and $D_{Ga}^{Cpx/melt}$ = 0.40), high-*P* (3 GPa) garnet peridotite melting ($D_{Ga}^{Opx/melt}$ = 0.38 and $D_{Ga}^{Cpx/melt}$ = 0.37), high-*P* (4 GPa) garnet peridotite melting ($D_{Ga}^{Opx/melt}$ = 0.26 and $D_{Ga}^{Cpx/melt}$ = 0.30), and MORB-like eclogite melting at 2-3 GPa ($D_{Ga}^{Cpx/melt}$ = 0.78). Consistent with previous studies, we find that Ga is incompatible in olivine during low-*P* peridotite melting ($D_{Ga}^{Ol/melt}$ = 0.08). Using values from this study and from the literature, we support the hypothesis that the Ga, Ga/Sc, and Ti contents of most mantle-derived melts require garnet in their source, but that additional lithologies (e.g., metasomatic veins) may be necessary to explain the chemical variability of those melts. Here we also obtain Ge partition coefficients applicable to low-*P* peridotite melting of 0.67, 1.04, and 1.12 for $D_{Ge}^{Ol/melt}$, $D_{Ge}^{Opx/melt}$, and $D_{Ge}^{Cpx/melt}$, respectively. Lastly, in order to provide a comprehensive picture of FRTE, Ga, and Ge partitioning during mantle melting, we provide a complete set of recommended partitioning values, based on results from this study and from the literature, for all FRTEs, Ga, and Ge, relevant for partial melting of spinel and garnet peridotite, as well as for MORB-like eclogite.

Keywords: First-row transition elements (FRTEs) ;Copper (Cu); Gallium (Ga); Germanium (Ge); mineral/melt partitioning; melting; peridotite; pyroxenite; MORB

INTRODUCTION

Variations of elemental and isotopic compositions in primitive basalts reflect the presence of chemical heterogeneities in the mantle source beneath intraplate ocean islands, mid-ocean ridges, and arcs (e.g., Zindler and Hart 1986; Hofmann 1997; Eiler et al. 2000; Hofmann 2003; Herzberg 2006; Sobolev et al. 2007; Jackson and Dasgupta 2008; Mallik and Dasgupta 2012). These chemical heterogeneities have also been linked to mineralogical variations in the source. In particular, first-row transition elements (FRTEs: Sc, Ti, V, Cr, Mn, Fe, Co, Ni, Cu, and Zn) have been used to track the mineralogical composition of mantle sources because they are not as sensitive to melt extraction processes as highly incompatible elements and are less sensitive to crystal fractionation than most major elements. Thus, their concentrations in mantle-derived melts have been used as direct indicators of mantle source mineralogy (e.g., Humayun et al. 2004; Sobolev et al. 2005; Prytulak and Elliott 2007; Sobolev et al. 2007; Qin and Humayun 2008; Le Roux et al. 2010; Herzberg 2011; Le Roux et al. 2011; Davis et al. 2013). Additionally, Cu, V/Sc, Fe^{3+}/Fe^{2+}, and Zn/Fe have been used to constrain the redox states of melts and oxygen fugacity in the source of mantle-derived melts (Carmichael 1991; Canil and O' Neill 1996; Lee et al. 2005; Kelley and Cottrell 2009; Mallmann and O' Neill 2009; Lee et al. 2010; Lee et al. 2012). Davis et al. (2013) also showed that the combination of FRTEs with mildly incompatible to compatible elements such as Ga and Ge could help decipher mineralogical variations in the source of mantle-derived melts. For example, they showed that Ga and Sc are fractionated during

peridotite melting in the garnet field, and they suggested that high Ga/Sc in melts would reflect the presence of residual garnet in the source, which preferentially incorporates Sc over Ga.

In parallel, variations of redox-sensitive elements such as V, Fe, and S, in basalts have been used to show that most arc magmas are more oxidized than MORBs (e.g., Carmichael 1991; Ballhaus 1993; Canil 1999; Jugo 2009; Kelley and Cottrell 2009; Laubier et al. 2014; Richards 2014). Similarly, the concentration of Cu, which is a chalcophile element, in mantle-derived melts has been used as a proxy to trace the presence of sulfides in the upper mantle (Lee et al. 2012), as sulfide stability and the presence of S^{2-} (as opposed to S^{6+}) in melt is a function of oxygen fugacity (e.g., Carroll and Rutherford 1987; Wallace and Carmichael 1994; Jugo et al. 2005; Jugo et al. 2010; Jego and Dasgupta 2014). The oxygen fugacity of abyssal peridotites typically ranges from -2.5 to +0.5 log units relative to the quartz-fayalite-magnetite buffer (QFM) (Wood et al. 1990). Under these conditions, the dominant oxidation state of sulfur is S^{2-} (sulfide). However, at higher fO_2 (> QFM + 2), sulfides become unstable to form SO_4^{2-} sulfates (Jugo et al. 2010; Jego and Dasgupta 2014). Thus, an oxidized mantle wedge should not be able to retain as much Cu as a sulfide-bearing MORB source, because Cu is highly incompatible in mantle silicates (Fellows and Canil 2012; Lee et al. 2012; Liu et al. 2014).

Mineral/melt partition coefficients during mantle melting have been constrained through numerous studies for a number of FRTEs (e.g., Watson 1977; Hart and Davis 1978; Dunn 1987; Beattie et al. 1991; Ehlers et al. 1992; Kohn and Schofield 1994; Walter 1998; Pertermann et al. 2004; Mysen 2007; Mallmann and O' Neill 2009; Le Roux et al. 2011; Davis et al. 2013). However, the partitioning behaviors of transition metal Cu, as well as post-transition metal Ga and metalloid Ge, are still uncertain. Here we provide new Cu partition coefficient values between mantle minerals and basaltic melts applicable to low-*P* peridotite melting (1.5 - 2 GPa)

91 measured in experiments of Le Roux et al. (2011), and we discuss possible reasons for
92 discrepancies between recent studies (Fellows and Canil 2012; Lee et al. 2012; Yao et al. 2012;
93 Liu et al. 2014). We also provide new Ga and Ge partition coefficient values, which have only
94 been constrained in a limited number of studies (Malvin and Drake 1987; Davis et al. 2013).
95 Combined with recent results for low-*P* (≤ 2 GPa) peridotite melting (Le Roux et al. 2011;
96 Fellows and Canil 2012; Lee et al. 2012; Yao et al. 2012; Liu et al. 2014), high-*P* (≥ 3 GPa)
97 peridotite melting (Davis et al. 2013; Liu et al. 2014), and MORB-like eclogite melting
98 (Pertermann et al. 2004), results from this study provide estimates of appropriate olivine-melt,
99 clinopyroxene-melt, and orthopyroxene-melt *D*s for Cu, Ga, and Ge, and a more comprehensive
100 picture of combined FRTE, Ga, and Ge partitioning during mantle melting. In a similar approach
101 to combining rare earth elements to decipher melt processes in the mantle, the combination of
102 FRTE, Ga, and Ge concentrations in mantle-derived melts can help decipher variations of source
103 mineralogy in the mantle.

104 **STARTING MATERIAL AND ANALYTICAL PROCEDURES**

105

106 The partitioning data reported here derive from the experiments described in Le Roux et
107 al. (2011), where detailed procedures can be found. The experimental and analytical procedures
108 used in that study are briefly mentioned here for completeness. Three different starting materials
109 were doped with variable amount of Cu, Ga, and Ge. Mix1 is a mixture between natural mid-
110 Atlantic ridge (MAR) basalt (~70 %) and KLB-1 peridotite (~30 %) that contains 597 ppm Cu,
111 1.3 ppm Ga, and 1380 ppm Ge. Mix2 is a MAR basalt that contains 1108 ppm Cu, 2200 ppm Ga,
112 and 2750 ppm Ge. Mix3 is a synthetic basalt reconstructed using reagent grade oxide powders
113 that contains 1172 ppm Cu, 1248 ppm Ga, and 1624 ppm Ge.

Partitioning experiments were carried out using an end-loaded piston cylinder device at Rice University (USA), following the pressure-temperature calibration of Tsuno and Dasgupta (2011). Starting mixes were contained in graphite capsules at temperature and pressure conditions varied from 1290 °C to 1500 °C and 1.5 GPa to 2 GPa. The use of graphite capsules promotes reducing conditions where the dominant valence state of Cu, Ga, and Ge should be +1, +3, and +4, respectively (Capobianco et al. 1999; Liu et al. 2014).

Copper, Ga, and Ge concentrations in olivine, orthopyroxene, clinopyroxene, and melt were measured using an electron probe micro-analyzer (EPMA) CAMECA SX-50 at Texas A&M University (USA). Cu, Ga, and Ge concentrations were measured by EPMA using an accelerating voltage of 20 kV, a beam current of 300 nA and 60 s peak counting time. The beam diameter used to measure silicates was 1–3 μm and ~20 μm for quenched melts. The detection limits were estimated to be 14, 23, and 31 $\mu g.g^{-1}$ for Cu, Ga, and Ge, respectively, in olivine, and 21, 33, 45 $\mu g.g^{-1}$ for Cu, Ga, and Ge, respectively, in melts. All reported values have at least twice the detection limit values. The quality of EPMA data was tested by re-analyzing large grains and quenched melts using laser ablation inductively coupled plasma mass spectrometry (LA-ICP-MS) with a Thermo-Finnigan Element Sector ICP-MS coupled with a New Wave 213 nm laser ablation system at Rice University (USA). ^{63}Cu, ^{69}Ga, ^{73}Ge and ^{74}Ge concentrations were measured by LA-ICP-MS in medium mass resolution mode ($m/\delta m=3000$). ^{73}Ge and ^{74}Ge gave similar results. We used a 100-μm laser spot to measure Cu, Ga, and Ge concentrations in experimental charges and a 55-μm laser spot in external standards. The energy density ranged between 15 and 20 J/cm^2 and the repetition rate was 10 Hz. Sensitivity was estimated at about 350,000 cps/ppm for La on a BHVO2 glass standard using a 55-μm laser beam at 10 Hz (15.6 ppm of La; Gao et al. 2002). The external reproducibility and accuracy of the measurements

were checked using BHVO2G, BCR2G and NIST610 standards. Correlations between EPMA and LA-ICP-MS measurements are presented in Figure 1. EPMA data were used to calculate the partition coefficients presented in this study.

RESULTS

Phase assemblage and approach to equilibrium

Experiments from Le Roux et al. (2011) yielded mineral assemblages that contain the following phases: Melt ± Olivine (Ol) ± Orthopyroxene (Opx) ± Clinopyroxene (Cpx). Phase assemblages and major element compositions of minerals are reported in le Roux et al. (2011). The major element compositions of minerals fall within the range of previously reported compositions for mantle minerals in experiments performed at similar experimental conditions (e.g., Kinzler and Grove 1992; Kinzler 1997; Kogiso et al. 1998; Wasylenki et al. 2003; Falloon et al. 2008), although pyroxenes are richer in Al_2O_3 than in natural spinel peridotites (e.g., Le Roux et al. 2007).

Approach to equilibrium is supported by textural evidence such as relatively homogeneous olivine size (≤ 50–70 μm) and pyroxene size (≤ 30 μm) within individual experiments, and 120º angles identified at three-grain junctions. Approach to equilibrium is also supported by chemical evidence, such as analytical consistency between single grains in individual experiments, no discernible zoning on scanning electron microscope images, and exchange partition coefficient $K_{D\ Fe/Mg}$ between olivine and melt ($= (X_{ol}^{Fe2+} / X_{melt}^{Fe2+}) / (X_{Ol}^{Mg2+} / X_{melt}^{Mg2+})$) ranging from 0.33 to 0.35, which is in good agreement with previous values obtained in similar experimental conditions (Roeder and Emslie 1970; Kushiro and Walter 1998;

159 Walter 1998; Kushiro 2001; Toplis 2005). The measured $K_{D\ Fe/Mg}$ between orthopyroxene and
160 basaltic melt range between 0.29 and 0.36, which is also consistent with previous experimental
161 studies (e.g., Kinzler and Grove 1992; Walter 1998; Parman and Grove 2004). Finally, the
162 residual squares of the mass balance (calculated by using the major element compositions of all
163 phases and the modal proportions that give minimum residual squares) are consistent with a
164 closed system in terms of major elements.
165

166 **Data quality**

167 **Measurements.** Copper, gallium, and germanium concentrations were measured by both
168 EPMA and LA-ICP-MS in six glasses and one clinopyroxene (Fig. 1). Our comparison was
169 performed using mineral and glasses that have significant amounts of trace elements (> 500
170 ppm), while some of our minerals have trace element concentrations below 100 ppm. We note
171 that previous studies have reported large discrepancies between EPMA and LA-ICP-MS
172 measurements at concentrations of 100 ppm of lower (Fellows and Canil 2012; Liu et al. 2014).
173 However, previous studies used standard analytical settings such as lower currents of 10 to 40
174 nA (instead of 300 nA) and shorter counting times of 20 to 40 s. (instead of 60 s.), which led to
175 detection limits significantly higher than what we report here. For example, Cu detection limit is
176 14 ppm in this study, and 380 ppm in Fellows and Canil (2012) study. Within analytical
177 uncertainty, Cu measurements plot on a 1:1 correlation line. Gallium concentrations in two
178 quenched melts and one clinopyroxene are higher, and lower, by EPMA than by LA-ICP-MS,
179 respectively. Although the number of measurements is limited, this could indicate that Ga
180 partition coefficients calculated with EPMA data are slightly under-estimated. Germanium
181 concentrations are higher when measured with EPMA than with LA-ICP-MS. However, because

partition coefficients have been calculated from elemental concentrations in melts and minerals both obtained by EPMA, any discrepancy should be canceled out during partition coefficient calculations.

Elemental losses. Cu loss has been associated with Fe loss in Pt and graphite-lined Pt capsule experiments (Fellows and Canil 2012), because Cu and Fe diffuse through the graphite capsule and alloy with the Pt outer capsule. Although we did not use Pt outer capsules in this study, we calculated Fe, Cu, Ga, and Ge losses by mass balance between concentrations in starting materials (bulk glass) and concentrations in run products multiplied by phase fractions (Le Roux et al. 2011), in experiments where all phases have been analyzed (Table 1). Ge concentrations in the bulk glass made of starting material Mix 1 were significantly lower than Ge concentrations obtained in minerals and melts, yielding inconsistent gains of > 400 % Ge. Because Ge may have been heterogeneously distributed in starting material Mix 1 as it was the last element added to the mixture, we calculated Ge loss/gain by using Ge concentrations of starting material Mix 1 obtained from weighing.

Two experiments have lost more than 50 % Cu, and six experiments have lost less than 40 % Cu. Fe loss/gain is very limited (< 7 %) and there is no correlation between Fe loss and Cu loss. Kiseeva and Wood (2013) observed that graphite capsule experiments run for seven hours at 1400ºC and 1.5 GPa show less than 10 % Cu loss. Here, we observe a large range of Cu loss in experiments that run for 20 hours or more (- 13 % to – 73 %), but we do not observe systematic correlations between Cu loss and duration or temperature. We suggest that Cu loss occurred through formation of Cu-carbonyl complexes due to the presence of graphite. We also observe a positive correlation between $D_{Cu}^{Opx/melt}$ and Cu loss (Fig. 2). As elements diffuse faster through melt than through minerals (Zhang 2010), diffusion of Cu from the melt to the graphite capsule

could lead to Cu depletion in the melt. This means that partition coefficients measured in experiments where large Cu losses occurred could be slightly over-estimated. On the other hand, Ga and Ge losses appear limited.

Henrian behavior. Similar to Fellows and Canil (2012) and Liu et al. (2014), our experiments were doped beyond typical Cu, Ga, and Ge concentrations in mantle minerals. The partitioning behavior of trace elements in natural minerals obeys Henry's law, which means that the value of partition coefficient is independent of the element's concentration in mineral or melt. If Henry's law is obeyed, there is no correlation between partition coefficients and elemental concentrations in minerals or melts. In this study, we used different starting materials and ran the experiments over a range of *P*-*T* conditions, which will affect partition coefficient values. Thus, correlations between partition coefficients and elemental concentrations could reflect other factors than a non-henrian behavior. Although we do not observe correlations between partition coefficients of Ga and Ge against their concentrations in run products, $D_{Cu}^{Cpx/melt}$ increases with increasing Cu content of clinopyroxene (Fig. 3a). A similar positive correlation is observed for the 'MORB' experiments reported in Liu et al. (2014), but the increase was attributed to the compositional dependence of $D_{Cu}^{Cpx/melt}$ on Na_2O content of clinopyroxene (Fig. 3b). Below, we discuss the effects of temperature and mineral compositions on partitioning values, and the possibility of a non-henrian behavior of Cu during partitioning between clinopyroxene and melt.

Effects of temperature and composition on partition coefficients

Trace element partitioning between mantle silicates and melt may depend on pressure, temperature, composition of melt and minerals, and oxygen fugacity (e.g., Wood and Blundy 2003). Liu et al. (2014) have suggested that fO_2, which should be the same in all of our

experiments, exerts the main control on $D_{Cu}^{Ol/melt}$ and $D_{Cu}^{Opx/melt}$. Average partition coefficients from this study are reported in Table 2. We observe no correlation between $D_{Cu}^{Ol/melt}$, $D_{Cu}^{Opx/melt}$ and temperature or composition. Liu et al. (2014) suggested that $D_{Cu}^{Cpx/melt}$ is mostly controlled by Na_2O content of clinopyroxene as Cu^+ could substitute for Na^+ in the crystal lattice. Here we observe a rough correlation between $D_{Cu}^{Cpx/melt}$ and Na_2O content of clinopyroxene (Fig. 3b). It is unclear if the correlation reflects a non-henrian behavior, or the fact that clinopyroxene were produced with different starting materials than in Liu et al. (2014), producing a different slope for the correlation. Thus, we suggest that our lowest $D_{Cu}^{Cpx/melt}$ value (0.09) is more conservative than the average $D_{Cu}^{Cpx/melt}$ value to model mantle melting.

It has been shown that $D_{Ga}^{Ol/melt}$, $D_{Ga}^{Opx/melt}$, and $D_{Ga}^{Cpx/melt}$ positively correlate with the Al_2O_3 content of olivine, orthopyroxene, and clinopyroxene, respectively. Davis et al. (2013) hypothesized that this correlation probably reflects the fact that Ga^{3+} and Al^{3+} have similar ionic radii in octahedral coordination (0.62Å and 0.535Å respectively). By combining our results with previous studies (Malvin and Drake 1987; Hart and Dunn 1993; Mallmann and O' Neill 2009; Davis et al. 2013), we observe a tight correlation between the Al_2O_3 content of orthopyroxene and clinopyroxene, and $D_{Ga}^{Opx/melt}$ and $D_{Ga}^{Cpx/melt}$, respectively (Fig. 4). Lastly, we observe a moderate decrease of $D_{Ge}^{Opx/melt}$ with increasing temperature (Fig. 5).

DISCUSSION

Comparison with previous studies

Because Cu, Ga, and Ge concentrations in mantle-derived melts may trace igneous processes in the Earth's mantle, it is critical to constrain their partitioning behaviors during

mantle melting, considering variations in source lithologies and fO_2. However, Ga and Ge partition coefficients are only constrained by a limited number of studies (e.g., Davis et al. 2013), and in the case of Cu, data variability is complicated to interpret (Fellows and Canil 2012; Lee et al. 2012; Liu et al. 2014). Here we compare our results with previously published studies and, in the case of Cu, we discuss the reasons for partition coefficient variations between studies.

Copper. Cu partition coefficients presented in previous studies (Fig. 6a) span a large range of values (Hart and Dunn 1993; Gaetani and Grove 1997; Fellows and Canil 2012; Lee et al. 2012; Yao et al. 2012; Liu et al. 2014). Two of our experiments yield low $D_{Cu}^{Ol/melt}$ values ($\leq$ 0.09) that are consistent with recent studies (Fellows and Canil 2012; Lee et al. 2012; Liu et al. 2014), however two other experiments yield high $D_{Cu}^{Ol/melt}$ values ($\geq$ 0.17). Similar to Liu et al. (2014), we observe no correlation between $D_{Cu}^{Ol/melt}$ and olivine composition. We also observe no effect of temperature, pressure, or Cu loss. Although fO_2 is probably the main parameter that controls $D_{Cu}^{Ol/melt}$, Liu et al. (2014) reported variable $D_{Cu}^{Ol/melt}$ values at high oxygen fugacities (> QFM + 3), from 0.074 to 0.143. Their lowest value obtained in oxidizing conditions (0.074) is very close to the average value of 0.05 obtained in reducing conditions (QFM $\leq$ + 1.2), which means that fO_2 may not be the sole parameter that controls $D_{Cu}^{Ol/melt}$. Compared to partition coefficients obtained between groundmass and minerals (Lee et al. 2012), experimental D_{Cu} are usually equivalent or higher (Gaetani and Grove 1997; Fellows and Canil 2012; Yao et al. 2012; Liu et al. 2014). In order to define a maximum value for $D_{Cu}^{Ol/melt}$ applicable to low-*P* peridotite melting in relatively reducing conditions, we consider an olivine in equilibrium with a MORB that contains 80 ppm Cu (Lee et al. 2012). As measured in Lee et al. (2012), olivine could contain as much as ~11-12 ppm Cu, although most olivines contained less than 4 ppm Cu. Thus,

$D_{Cu}^{Ol/melt}$ of 0.15 would be an absolute upper value to model low-*P* peridotite melting in relatively reducing conditions (QFM < 1.5). $D_{Cu}^{Opx/melt}$ from this study are within the range of values reported in previous studies, but higher than $D_{Cu}^{Opx/melt}$ in Lee et al. (2012), Yao et al. (2012) and Liu et al. (2014), and lower than $D_{Cu}^{Opx/melt}$ in Fellows and Canil (2012). However, $D_{Cu}^{Opx/melt}$ of 0.15 used in Fellows and Canil (2012) has been obtained with analyses that were reported by the authors to be below detection limits (experiment P386), thus it is unclear how appropriate this value is. Given the same assumptions about Cu content in the MORB source and using inter-mineral partition coefficients (Fig. 7a), an absolute upper value for $D_{Cu}^{Opx/melt}$ applicable to mantle melting in relatively reducing conditions is 0.13 (= max. $D_{Cu}^{Ol/melt}$ × Cu_{Opx} / Cu_{Ol}), which is just above the value that we obtain here. $D_{Cu}^{Cpx/melt}$ also spans a large range of values, which may be attributed to a dependence of $D_{Cu}^{Cpx/melt}$ on Na_2O clinopyroxene content and/or a non-henrian behavior (Fig. 3), as suggested by Liu et al. (2014). The preferred value for $D_{Cu}^{Cpx/melt}$ (0.06) obtained in reducing conditions in Liu et al. (2014) had been calculated from experiment 'komatiite-L4' that had the lowest amount of Na_2O in clinopyroxene. The average $D_{Cu}^{Cpx/melt}$ for all experiments performed in reducing conditions in Liu et al. (2014) is 0.09±0.04. Using inter-mineral partition coefficients (Fig. 7b), we calculate that an absolute upper value for $D_{Cu}^{Cpx/melt}$ applicable to low-*P* peridotite melting would be 0.16. In Table 3, we report $D_{Cu}^{Mineral/melt}$ from this study and from the literature. Our $D_{Cu}^{Mineral/melt}$ values are within error of, and on average higher than, values reported in previous studies for olivine (Fellows and Canil 2012; Lee et al. 2012; Liu et al. 2014) and clinopyroxene (Lee et al. 2012; Liu et al. 2014). For comparison with our data, we have reported in Table 3 the lower range of $D_{Cu}^{Mineral/melt}$ from

recent studies, suitable to model low-*P* peridotite melting at QFM < 1.5. The reason for differences between studies is a combination of compositional control on partitioning (e.g. Na_2O in clinopyroxene), effect of oxygen fugacity, and may also be linked to some elemental loss, non-henrian behavior for experiments with high trace element concentrations, and/or incomplete chemical equilibrium.

Gallium. Our results confirm that Ga is incompatible in olivine and moderately incompatible to compatible in pyroxenes (Malvin and Drake 1987; Mallmann and O' Neill 2009; Davis et al. 2013). Because Al-content of pyroxenes exert the strongest control on $D_{Ga}^{Px/melt}$ (Davis et al. 2013), using data from this study and those from previous studies over a range of *P*-*T* conditions (Malvin and Drake 1987; Hart and Dunn 1993; Mallmann and O' Neill 2009; Davis et al. 2013), we derive parameterizations to predict $D_{Ga}^{Px/melt}$ as a function of pyroxene compositions for both peridotitic and eclogitic systems (Fig. 4). We find that $D_{Ga}^{Cpx/melt} = 0.002x^2 + 0.014x + 0.202$, and $D_{Ga}^{Opx/melt} = 0.0016x^2 + 0.039x + 0.0563$, where x is Al_2O_3 wt. % in clinopyroxene and orthopyroxene, respectively. The Al content of peridotitic pyroxene strongly depends on *P*. It increases steadily up to 2.8 GPa, where it starts decreasing owing to the stability of garnet (e.g., Hirschmann et al. 2009). Our parameterizations cover Al_2O_3 content between ~2 and ~14 wt.% for Cpx and ~1 and ~9 wt.% for Opx. This allows us to use $D_{Ga}^{Px/melt}$ values that are appropriate for lithology of interest (pyroxenes in high-alumina lithology such as eclogite and pyroxenes in low-alumina lithology such as peridotite) and *P*-*T* conditions of interest (low-*P* versus high-*P*) that, in turn, influences pyroxene compositions. We use the parameterization of Hirschmann et al. (2009) to derive representative Al_2O_3 content of peridotitic pyroxenes at 1.5 GPa (3.8 wt. %), 2.8 GPa (7.3 wt. %) and 4 GPa (4.4 wt. %). We assume that Cpx and Opx have similar Al content (Hirschmann et al. 2009). For pyroxenitic clinopyroxenes,

315 we use the average Al_2O_3 content of clinopyroxenes from Pertermann and Hirschmann (2003a),
316 i.e. 14.4 wt. %. Using our parameterization (Fig. 4), we suggest that appropriate $D_{Ga}^{Opx/melt}$ for
317 low-*P* spinel peridotite melting (1.5 GPa), intermediate-P spinel peridotite (2.8 GPa), high-*P*
318 garnet peridotite melting (3 GPa), and high-*P* garnet peridotite melting (4 GPa) are 0.23, 0.42,
319 0.38, and 0.26, respectively. Similarly, we suggest that appropriate $D_{Ga}^{Cpx/melt}$ for low-*P* spinel
320 peridotite melting (1.5 GPa), intermediate-P spinel peridotite (2.8 GPa), high-*P* garnet peridotite
321 melting (3 GPa), high-*P* garnet peridotite melting (4 GPa), and MORB-like eclogite melting (2-3
322 GPa) are 0.28, 0.40, 0.37, 0.30, and 0.78, respectively.

323 **Germanium.** Within uncertainty, $D_{Ge}^{Opx/melt}$ and $D_{Ge}^{Cpx/melt}$ from Davis et al. (2013)
324 overlap with our data, but their average values are slightly lower (Fig. 6). $D_{Ge}^{Opx/melt}$ obtained in
325 this study show a positive correlation with TiO_2 content of orthopyroxene (not shown). However,
326 the correlation is not observed in Davis et al. (2013). Although various starting materials have
327 been used, we also observe a moderate decrease of $D_{Ge}^{Opx/melt}$ with increasing temperature (Fig.
328 5). Average $D_{Ge}^{Ol/melt}$ from Davis et al. (2013) is also lower than our average value. Experiments
329 in Davis et al. (2013) were conducted at higher pressure (3 GPa), while Malvin and Drake (1987)
330 study was performed at atmospheric pressure. The variability of $D_{Ge}^{Cpx/melt}$ may thus reflect an
331 effect of pressure on Ge partitioning. We did not observe any dependence of $D_{Ge}^{Cpx/melt}$ and
332 $D_{Ge}^{Ol/melt}$ on temperature or mineral composition.

IMPLICATIONS

Cu partitioning in the mantle and Cu content of MORB

Partition coefficients from this study confirm that Cu is highly incompatible in mantle minerals and is mostly controlled by sulfides during MORB melting (Lee et al. 2012; Liu et al. 2014). To illustrate this, we calculate the Cu content of peridotite-derived melts using partition coefficients from this study (Table 3) and from the literature (Fig. 8). During near-fractional melting in the MORB source, batch melts are removed at small increments and the composition of the peridotite residue is updated accordingly. The aggregated melt composition is reported. We assume that the DMM source contains 30 µg/g Cu (Sun 1982; Salters and Stracke 2004) and ~ 200 µg/g S (Chaussidon et al. 1989; Lorand 1991; O'Neill 1991; Lee et al. 2012; Nielsen et al. 2014), and that MORB melts correspond to a mean extent of melting of ~ 5 to 15 % of DMM (Johnson et al. 1990; Kinzler and Grove 1992; Langmuir et al. 1992; Workman and Hart 2005). The assumed mineralogy of the sulfide-free source is 57 % olivine, 28 % orthopyroxene, 13 % clinopyroxene, 2 % spinel (Workman and Hart 2005) and the assumed mineralogy of the sulfide-bearing source is 56.97 % olivine, 27.98 % orthopyroxene, 12.99 % clinopyroxene, 2 % spinel and 0.06 % sulfides (Lee et al. 2012). In Figure 8a, where initial $D^{peridotite/melt}$ varies from 0.12 (this study) to 0.05 (Lee et al. 2012; Liu et al. 2014), a sulfide-free peridotite source cannot reproduce the Cu content of primitive MORBs. On the other hand, the Cu content of primitive MORBs can be reproduced by melting of a sulfide-bearing peridotite source (Fig. 8b) using initial $D^{peridotite/melt}$ ranging from ~0.60 (this study) to ~0.5 (Lee et al. 2012). We assume $D_{Cu}^{sf/melt}$ = 800, which means that Cu is moderately incompatible at the beginning of melting but becomes highly incompatible as progressive melting leads to the depletion of S (and sulfide) in the peridotite residue (Ripley et al. 2002). The rate of S depletion in the residue depends on the

356 solubility of S in the melt, which increases with increasing *T* and decreasing *P***.** Details of
357 melting calculations for sulfides are provided in the supplementary material of Lee et al. (2012).
358

359 **Garnet in the mantle source and its effect on the Ga content of mantle-derived melts**

360 Davis et al. (2013) suggested that high Ga /Sc contents of mantle-derived melts reflect
361 the presence of garnet in their source because Ga is strongly compatible in spinel but
362 incompatible in garnet, whereas Sc is strongly compatible in garnet but incompatible in spinel
363 (see summary of Davis et al. 2013 values in Table 3). Also, Prytulak and Elliott (2007) have
364 suggested that elevated Ti in mantle-derived melts could not be produced by a source solely
365 composed of peridotite. Here we compare the Ga, Ti, and Ga/Sc contents of primitive mantle-
366 derived melts (MgO > 8 wt. %) with the composition of model melts produced by near fractional
367 melting of various mantle sources using recommended Ga values from this study, which takes
368 into account the dependence of Ga partitioning between pyroxenes and melt on the Al_2O_3 content
369 of pyroxenes (Fig. 4; Table 3). To model low-*P* near-fractional melting of spinel peridotite (1-2
370 GPa), high-*P* near-fractional melting of garnet peridotite (3-4 GPa), and MORB-like eclogite
371 melting (2-3 GPa) we assume that the starting mineralogy is 57 % Ol, 28 % Opx, 13 % Cpx and
372 2 % Sp (Workman and Hart 2005), 60 % Ol, 16 % Opx, 13 % Cpx and 11 % Gt (Ionov 2004),
373 and 80 % Cpx and 20 % Gt (Pertermann and Hirschmann 2003b), respectively. We use the
374 melting reaction of Wasylenki et al. (2003) to model spinel peridotite melting (0.571 Opx +
375 0.735 Cpx + 0.041 Sp = 0.347 Ol + 1 liquid), the melting reaction of Walter (1998) to model
376 garnet peridotite melting (0.08 Ol + 0.81 Cpx + 0.3 Gt = 0.19 Opx + 1 liquid), and the melting
377 reaction of Pertermann and Hirschmann (2003a) to model MORB-like eclogite melting (0.84
378 Cpx + 0.16 Gt = 1 liquid). We assume that the peridotite source contains 798 µg/g Ti, 3.2 µg/g

379 Ga, and 16.3 μg/g Sc (Salters and Stracke 2004), and that the pyroxenite source contains 8500
380 μg/g Ti, 21 μg/g Ga, and 36.8 μg/g Sc (Arevalo and McDonough 2010). In Figure 9, we show
381 that the Ga, Ti, and Ga/Sc contents of mantle-derived melt increase with increasing garnet
382 content of the source. The trend supports the hypothesis that garnet is likely present in the source
383 of a number of intraplate and ocean island melts, as well as in MORB (e.g., Salters and Hart
384 1989; McKenzie and O'Nions 1995; Bourdon et al. 1996; Hirschmann and Stolper 1996; Eiler et
385 al. 2000; Prytulak and Elliott 2007; Elkins et al. 2008). However, Ga, Ti, and Ga/Sc variations in
386 mantle-derived melts cannot be solely explained by melting of a peridotite source, or mixing
387 between peridotite and eclogite-derived melts. For example, we show that the elevated Ti content
388 of some intraplate volcanics and ocean island basalts is associated with lower Ga content than
389 what would be produced by melting of MORB-like eclogite. Thus, additional lithologies must be
390 present in the source to explain the Ga, Ti, and Ga/Sc systematics of Ti-enriched melts. Although
391 partition coefficients for sediment/melt or metasomatic veins /melt are not available for elements
392 like Ga or Ge, we suggest that exotic lithologies may affect the Ga, Ge, and Ga/Sc of mantle-
393 derived melts. For example, Ge/Si ratios may experience strong fractionations during
394 weathering, biogenic precipitation of silica, or hydrothermal alteration (e.g., Kurtz et al. 2002;
395 Shen et al. 2011). However, these predictions cannot be tested at this point, due to the lack of
396 partition coefficients and the scarcity of Ge measurements in mantle-derived melts.

397 **FRTEs, Ga and Ge during mantle melting**

398 This study provides additional constraints for the partitioning behavior of Cu, Ga, and Ge
399 during mantle melting. Using results from this study and the literature, we use a set of
400 partitioning values for all FRTEs, Ga, and Ge, during peridotite and MORB-like eclogite melting
401 (Table 3) that allows us to place those elements with respect to other FRTEs (Fig. 10). Table 3

preferentially reports studies performed at experimental conditions applicable to peridotite melting in relatively reducing conditions (QFM < 1.5), where partition coefficients have been obtained for multiple elements, in order to ease comparison between partition coefficients. Similar to REE patterns, the full spectrum of elements can be used to fingerprint the source of basalts, with the difference that FRTEs, Ga, and Ge are more sensitive to source mineralogy, unlike highly incompatible elements, which are sensitive to degree of melting and melt or fluid metasomatism. Thus, the full spectrum of FRTEs, Ga, and Ge partition coefficients allows identification of elements most likely to trace pyroxene-dominated melting, or the presence of garnet in the source. For example, by comparing $D^{sp\ peridotite/melt}$ and $D^{gt\ peridotite/melt}$, one can anticipate that ratios of elements that negatively correlate with the garnet content of the source (e.g., Ga/Sc, Ti/Sc, Ga/Cr etc.) may be more likely to be elevated in mantle melts derived from a garnet-bearing peridotite compared to spinel-bearing peridotite. Depending on the concentrations of these elements in the source, the melting degree of the source, and the difference in partition coefficients between peridotite and pyroxenite, one can use those values to predict preferential enrichment or depletion throughout the entire set of elements presented here.

Acknowledgments

The authors thank Fred Davis and Dante Canil for their constructive reviews, and Ray Guillemette for his assistance with electron microprobe analyses at Texas A&M University. This study was supported by NSF-EAR 1220440 to VLR and NSF-EAR 1255391 to RD. VLR also received support from the Deep Ocean Exploration Institute at WHOI and the Penzance Endowed Fund in Support of Assistant Scientists.

References

Arevalo, R., and McDonough, W.F. (2010) Chemical variations and regional diversity observed in MORB. Chemical Geology, 271, 70-85.

Ballhaus, C. (1993) Redox states of lithospheric and asthenospheric upper-mantle. Contributions to Mineralogy and Petrology, 114, 331-348.

Barrie, C.T., Corfu, F., Davis, P., Coutts, A.C., and MacEachern, D. (1999) Geochemistry of the Dundonald komatiite-basalt suite and genesis of Dundeal Ni deposit, Abitibi subprovince, Canada. Economic Geology and the Bulletin of the Society of Economic Geologists, 94, 845-866.

Beattie, P., Ford, C., and Russell, D. (1991) Partition coefficients for olivine-melt and orthopyroxene-melt systems. Contributions to Mineralogy and Petrology, 109, 212-224.

Bourdon, B., Zindler, A., Elliott, T., and Langmuir, C.H. (1996) Constraints on mantle melting at mid-ocean ridges from global U-238-Th-230 disequilibrium data. Nature, 384, 231-235.

Briand, B., Bouchardon, J.L., Capiez, P., and Piboule, M. (2002) Felsic (A-type)-basic (plume-induced) Early Palaeozoic bimodal magmatism in the Maures Massif (southeastern France). Geological Magazine, 139, 291-311.

Canil, D. (1999) Vanadium partitioning between orthopyroxene, spinel and silicate melt and the redox states of mantle source regions for primary magmas. Geochimica Et Cosmochimica Acta, 63, 557-572.

Canil, D., and Fedortchouk, Y. (2000) Clinopyroxene-liquid partitioning for vanadium and the oxygen fugacity during formation of cratonic and oceanic mantle lithosphere. Journal of Geophysical Research-Solid Earth, 105, 26003-26016.

-. (2001) Olivine-liquid partitioning of vanadium and other trace elements, with applications to modern and ancient picrites. Canadian Mineralogist, 39, 319-330.

Canil, D., and O' Neill, H.S.C. (1996) Distribution of ferric iron in some upper-mantle assemblages. Journal of Petrology, 37, 609-635.

Capobianco, C.J., Drake, M.J., and de'Aro, J. (1999) Siderophile geochemistry of Ga, Ge, and Sn: Cationic oxidation states in silicate melts and the effect of composition in iron-nickel alloys. Geochimica Et Cosmochimica Acta, 63, 2667-2677.

Carmichael, I.S.E. (1991) The redox states of basic and silicic magmas - a reflection of their source regions. Contributions to Mineralogy and Petrology, 106, 129-141.

Carroll, M.R., and Rutherford, M.J. (1987) The stability of igneous anhydrite - experimental results and implications for sulfur behavior in the 1982 El-Chichon trachyandesite and other evolved magmas. Journal of Petrology, 28, 781-801.

Chaussidon, M., Albarede, F., and Sheppard, S.M.F. (1989) Sulfur isotope variations in the mantle from ion microprobe analyses of micro-sulfide inclusions. Earth and Planetary Science Letters, 92, 144-156.

Davis, F.A., Humayun, M., Hirschmann, M.M., and Cooper, R.S. (2013) Experimentally determined mineral/melt partitioning of first-row transition elements (FRTE) during partial melting of peridotite at 3 GPa. Geochimica Et Cosmochimica Acta, 104, 232-260.

Dunn, T. (1987) Partitioning of Hf, Lu, Ti and Mn between Olivine, Clinopyroxene and basaltic liquid Contributions to Mineralogy and Petrology, 96, 476-484.

Ehlers, K., Grove, T.L., Sisson, T.W., Recca, S.I., and Zervas, D.A. (1992) The effect of oxygen fugacity on the partitioning of nickel and cobalt between olivine, silicate melt, and metal Geochimica Et Cosmochimica Acta, 56, 3733-3743.

Eiler, J.M., Schiano, P., Kitchen, N., and Stolper, E.M. (2000) Oxygen-isotype evidence for recycled crust in the sources of mid-ocean-ridge basalts. Nature, 403, 530-534.

Elkins, L.J., Gaetani, G.A., and Sims, K.W.W. (2008) Partitioning of U and Th during garnet pyroxenite partial melting: Constraints on the source of alkaline ocean island basalts. Earth and Planetary Science Letters, 265, 270-286.

Falloon, T.J., Green, D.H., Danyushevsky, L.V., and McNeill, A.W. (2008) The composition of near-solidus partial melts of fertile peridotite at 1 and 1.5 GPa: Implications for the petrogenesis of MORB. Journal of Petrology, 49, 591-613.

Fellows, S.A., and Canil, D. (2012) Experimental study of the partitioning of Cu during partial melting of Earth's mantle. Earth and Planetary Science Letters, 337, 133-143.

Gaetani, G.A., and Grove, T.L. (1997) Partitioning of moderately siderophile elements among olivine, silicate melt, and sulfide melt: Constraints on core formation in the Earth and Mars. Geochimica Et Cosmochimica Acta, 61, 1829-1846.

Gao, S., Liu, X.M., Yuan, H.L., Hattendorf, B., Gunther, D., Chen, L., and Hu, S.H. (2002) Determination of forty two major and trace elements in USGS and NIST SRM glasses by laser ablation-inductively coupled plasma-mass spectrometry. Geostand. Newsl., 26, 181-196.

Greene, A.R., Scoates, J.S., Weis, D., Nixon, G.T., and Kieffer, B. (2009) Melting History and Magmatic Evolution of Basalts and Picrites from the Accreted Wrangellia Oceanic Plateau, Vancouver Island, Canada. Journal of Petrology, 50, 467-505.

Hart, S.R., and Davis, K.E. (1978) Nickel partitioning between olivine and silicate melt Earth and Planetary Science Letters, 40, 203-219.

Hart, S.R., and Dunn, T. (1993) Experimental cpx/melt partitioning of 24 trace elements. Contributions to Mineralogy and Petrology, 113, 1-8.

Hartlaub, R.P., Heaman, L.M., Ashton, K.E., and Chacko, T. (2004) The Archean Murmac Bay Group: evidence for a giant archean rift in the Rae Province, Canada. Precambrian Research, 131, 345-372.

Herzberg, C. (2006) Petrology and thermal structure of the Hawaiian plume from Mauna Kea volcano. Nature, 444, 605-609.

-. (2011) Identification of Source Lithology in the Hawaiian and Canary Islands: Implications for Origins. Journal of Petrology, 52, 113-146.

Hirschmann, M.M., and Stolper, E.M. (1996) A possible role for garnet pyroxenite in the origin of the ''garnet signature'' in MORB. Contributions to Mineralogy and Petrology, 124, 185-208.

Hirschmann, M.M., Tenner, T., Aubaud, C., and Withers, A.C. (2009) Dehydration melting of nominally anhydrous mantle: The primacy of partitioning. Physics of the Earth and Planetary Interiors, 176, 54-68.

Hofmann, A.W. (1997) Mantle geochemistry: the message from oceanic volcanism. Nature, 385, 219-229.

Hofmann, A.W. (2003) Sampling mantle heterogeneity through oceanic basalts: isotopes and trace elements. In R.W. Carlson, Ed. The Mantle and Core - Treatise on Geochemistry Vol. 2, 2.

Humayun, M., Qin, L.P., and Norman, M.D. (2004) Geochemical evidence for excess iron in the mantle beneath Hawaii. Science, 306, 91-94.

Ionov, D. (2004) Chemical variations in peridotite xenoliths from Vitim, Siberia: Inferences for REE and Hf behaviour in the garnet-facies upper mantle. Journal of Petrology, 45, 343-367.

Jackson, M.G., and Dasgupta, R. (2008) Compositions of HIMU, EM1, and EM2 from global trends between radiogenic isotopes and major elements in ocean island basalts. Earth and Planetary Science Letters, 276, 175-186.

Jego, S., and Dasgupta, R. (2014) The Fate of Sulfur During Fluid-Present Melting of Subducting Basaltic Crust at Variable Oxygen Fugacity. Journal of Petrology, 55, 1019-1050.

Jenner, F.E., and O'Neill, H.S.C. (2012) Analysis of 60 elements in 616 ocean floor basaltic glasses. Geochemistry Geophysics Geosystems, 13, Q02005.

Johnson, K.T.M., Dick, H.J.B., and Shimizu, N. (1990) Melting in the oceanic upper mantle: an ion micropobe study of diopsides in abyssal peridotites. Journal of Geophysical Research, 95, 2661-2678.

Jugo, P.J. (2009) Sulfur content at sulfide saturation in oxidized magmas. Geology, 37, 415-418.

Jugo, P.J., Luth, R.W., and Richards, J.P. (2005) Experimental data on the speciation of sulfur as a function of oxygen fugacity in basaltic melts. Geochimica Et Cosmochimica Acta, 69, 497-503.

Jugo, P.J., Wilke, M., and Botcharnikov, R.E. (2010) Sulfur K-edge XANES analysis of natural and synthetic basaltic glasses: Implications for S speciation and S content as function of oxygen fugacity. Geochimica Et Cosmochimica Acta, 74, 5926-5938.

Kelley, K.A., and Cottrell, E. (2009) Water and the Oxidation State of Subduction Zone Magmas. Science, 325, 605-607.

Kinzler, R.J. (1997) Melting of mantle peridotite at pressures approaching the spinel to garnet transition: Application to mid-ocean ridge basalt petrogenesis. Journal of Geophysical Research, 102, 853-874.

Kinzler, R.J., and Grove, T.L. (1992) Primary magmas of mid-ocean ridge basalts .1. Experiments and methods Journal of Geophysical Research, 97, 6885-6906.

Kiseeva, E.S., and Wood, B.J. (2013) A simple model for chalcophile element partitioning between sulphide and silicate liquids with geochemical applications. Earth and Planetary Science Letters, 383, 68-81.

Kogiso, T., Hirose, K., and Takahashi, E. (1998) Melting experiments on homogeneous mixtures of peridotite and basalt: application to the genesis of ocean island basalts. Earth and Planetary Science Letters, 162, 45-61.

Kohn, S.C., and Schofield, P.F. (1994) The importance of melt composition in controlling trace-element behavior - an experimental study of Mn and Zn partitioning between forsterite and silicate melts. Chemical Geology, 117, 73-87.

Kurtz, A.C., Derry, L.A., and Chadwick, O.A. (2002) Germanium-silicon fractionation in the weathering environment. Geochimica Et Cosmochimica Acta, 66, 1525-1537.

Kushiro, I. (2001) Partial melting experiments on peridotite and origin of mid-ocean ridge basalt. Annual Review of Earth and Planetary Sciences, 29, 71-107.

Kushiro, I., and Walter, M.J. (1998) Mg-Fe partitioning between olivine and mafic-ultramafic melts. Geophysical Research Letters, 25, 2337-2340.

Langmuir, C.H., Klein, E.M., and Plank, T. (1992) Petrological Systematics of Mid-Ocean Ridge Basalts: Constraints on Melt Generation Beneath Ocean Ridges. Mantle Flow and Melt Generation at Mid-Ocean Ridges, p. 183-280. American Geophysical Union.

Laubier, M., Grove, T.L., and Langmuir, C.H. (2014) Trace element mineral/melt partitioning for basaltic and basaltic andesitic melts: An experimental and laser ICP-MS study with application to the oxidation state of mantle source regions. Earth and Planetary Science Letters, 392, 265-278.

Le Roux, V., Bodinier, J.L., Tommasi, A., Alard, O., Dautria, J.M., Vauchez, A., and Riches, A.J.V. (2007) The Lherz spinel lherzolite: Refertilized rather than pristine mantle. Earth and Planetary Science Letters, 259, 599-612.

Le Roux, V., Dasgupta, R., and Lee, C.T.A. (2011) Mineralogical heterogeneities in the Earth's mantle: Constraints from Mn, Co, Ni and Zn partitioning during partial melting. Earth and Planetary Science Letters, 307, 395-408.

Le Roux, V., Lee, C.T.A., and Turner, S.J. (2010) Zn/Fe systematics in mafic and ultramafic systems: implications for detecting major element heterogeneities in the Earth's mantle. Geochimica Et Cosmochimica Acta, 74, 2779-2796.

Lee, C.-T.A., Luffi, P., Le Roux, V., Dasgupta, R., Albarede, F., and Leeman, W.P. (2010) The redox state of arc mantle using Zn/Fe systematics. Nature, 468, 681-685.

Lee, C.T.A., Leeman, W.P., Canil, D., and Li, Z.X.A. (2005) Similar V/Sc systematics in MORB and arc basalts: Implications for the oxygen fugacities of their mantle source regions. Journal of Petrology, 46, 2313-2336.

Lee, C.T.A., Luffi, P., Chin, E.J., Bouchet, R., Dasgupta, R., Morton, D.M., Le Roux, V., Yin, Q.Z., and Jin, D. (2012) Copper systematics in arc Magmas and Implications for Crust-Mantle Differentiation. Science, 336, 64-68.

Liu, X.C., Xiong, X.L., Audetat, A., Li, Y., Song, M.S., Li, L., Sun, W.D., and Ding, X. (2014) Partitioning of copper between olivine, orthopyroxene, clinopyroxene, spinel, garnet and silicate melts at upper mantle conditions. Geochimica Et Cosmochimica Acta, 125, 1-22.

Lorand, J.P. (1991) Sulphide petrology and sulphur geochemistry of orogenic lherzolites: a comparative study of the Pyrenean bodies (France) and the Lanzo massif (Otaly). In M.A. Menzies, C. Dupuy, and A. Nicolas, Eds. Orogenic lherzolites and Mantle Processes, J. Petrol. Spec. Vol., p. 77-95.

Ma, G.S.K., Malpas, J., Xenophontos, C., and Chan, G.H.N. (2011) Petrogenesis of Latest Miocene-Quaternary Continental Intraplate Volcanism along the Northern Dead Sea Fault System (Al Ghab-Homs Volcanic Field), Western Syria: Evidence for Lithosphere-Asthenosphere Interaction. Journal of Petrology, 52, 401-430.

Mallik, A., and Dasgupta, R. (2012) Reaction between MORB-eclogite derived melts and fertile peridotite and generation of ocean island basalts. Earth and Planetary Science Letters, 329, 97-108.

Mallmann, G., and O' Neill, H.C. (2009) The Crystal/Melt partitioning of V during mantle melting as a function of oxygen fugacity compared with some other elements (Al, P, Ca, Sc,Ti, Cr, Fe, Ga,Y, Zr and Nb). Journal of Petrology, 50, 1765-1794.

Malvin, D.J., and Drake, M.J. (1987) Experimental determination of crystal/melt partitioning of Ga and Ge in the system forsterite-anorthite-diopside. Geochimica Et Cosmochimica Acta, 51, 2117-2128.

McDade, P., Blundy, J.D., and Wood, B.J. (2003) Trace element partitioning on the Tinaquillo Lherzolite solidus at 1.5 GPa. Physics of The Earth and Planetary Interiors, 139, 129-147.

McKenzie, D., and O'Nions, R.K. (1995) The source regions of ocean island basalts. Journal of Petrology, 36, 133-159.

Mysen, B. (2007) Partitioning of calcium, magnesium, and transition metals between olivine and melt governed by the structure of the silicate melt at ambient pressure. American Mineralogist, 92, 844-862.

Nielsen, S.G., Shimizu, N., Lee, C.-T.A., and Behn, M.D. (2014) Chalcophile behavior of thallium during MORB melting and implications for the sulfur content of the mantle. Geochemistry, Geophysics, Geosystems, 15, 4905-4919.

Ntaflos, T., and Richter, W. (2003) Geochemical constraints on the origin of the Continental Flood Basalt magmatism in Franz Josef Land, Arctic Russia. European Journal of Mineralogy, 15, 649-663.

O'Neill, H.S. (1991) The origin of the Moon and the early history of the Earth - a chemical model. 2. The Earth. Geochimica Et Cosmochimica Acta, 55, 1159-1172.

Parman, S.W., and Grove, T.L. (2004) Harzburgite melting with and without H2O: Experimental data and predictive modeling. Journal of Geophysical Research, 109, 20.

Pertermann, M., and Hirschmann, M.M. (2003a) Anhydrous partial melting experiments on MORB-like eclogite: Phase relations, phase compositions and mineral-melt partitioning of major elements at 2-3 GPa. Journal of Petrology, 44, 2173-2201.

-. (2003b) Partial melting experiments on a MORB-like pyroxenite between 2 and 3 GPa: Constraints on the presence of pyroxenite in basalt source regions from solidus location and melting rate. Journal of Geophysical Research, 108, 17.

Pertermann, M., Hirschmann, M.M., Hametner, K., Gunther, D., and Schmidt, M.W. (2004) Experimental determination of trace element partitioning between garnet and silica-rich liquid during anhydrous partial melting of MORB-like eclogite. Geochemistry Geophysics Geosystems, 5, 23.

Prytulak, J., and Elliott, T. (2007) TiO2 enrichment in ocean island basalts. Earth and Planetary Science Letters, 263, 388-403.

Qin, L.P., and Humayun, M. (2008) The Fe/Mn ratio in MORB and OIB determined by ICP-MS. Geochimica et Cosmochimica Acta, 72, 1660-1677.

Richards, J.P. (2014) The oxidation state, and sulfur and Cu contents of arc magmas: implications for metallogeny. Lithos.

Righter, K., Leeman, W.P., and Hervig, R.L. (2006) Partitioning of Ni, Co and V between spinel-structured oxides and silicate melts: Importance of spinel composition. Chemical Geology, 227, 1-25.

Ripley, E.M., Brophy, J.G., and Li, C.S. (2002) Copper solubility in a basaltic melt and sulfide liquid/silicate melt partition coefficients of Cu and Fe. Geochimica Et Cosmochimica Acta, 66, 2791-2800.

Roeder, P.L., and Emslie, R.F. (1970) Olivine-liquid equilibrium. Contributions to Mineralogy and Petrology, 29, 275-289.

Salters, V.J.M., and Hart, S.R. (1989) The hafnium paradox and the role of garnet in the source of mid-ocean ridge basalts. Nature, 342, 420-422.

Salters, V.J.M., and Stracke, A. (2004) Composition of the depleted mantle. Geochemistry Geophysics Geosystems, 5, 27.

Shen, B., Lee, C.T.A., and Xiao, S.H. (2011) Germanium/silica ratios in diagenetic chert nodules from the Ediacaran Doushantuo Formation, South China. Chemical Geology, 280, 323-335.

Sobolev, A.V., Hofmann, A.W., Kuzmin, D.V., Yaxley, G.M., Arndt, N.T., Chung, S.L., Danyushevsky, L.V., Elliott, T., Frey, F.A., Garcia, M.O., Gurenko, A.A., Kamenetsky, V.S., Kerr, A.C., Krivolutskaya, N.A., Matvienkov, V.V., Nikogosian, I.K., Rocholl, A., Sigurdsson, I.A., Sushchevskaya, N.M., and Teklay, M. (2007) The amount of recycled crust in sources of mantle-derived melts. Science, 316, 412-417.

Sobolev, A.V., Hofmann, A.W., Sobolev, S.V., and Nikogosian, I.K. (2005) An olivine-free mantle source of Hawaiian shield basalts. Nature, 434, 590-597.

Sun, S.S. (1982) Chemical composition and origin of the Earth's primitive mantle Geochimica et Cosmochimica Acta, 46, 179-192.

Toplis, M.J. (2005) The thermodynamics of iron and magnesium partitioning between olivine and liquid: criteria for assessing and predicting equilibrium in natural and experimental systems. Contributions to Mineralogy and Petrology, 149, 22-39.

Trua, T., Esperanca, S., and Mazzuoli, R. (1998) The evolution of the lithospheric mantle along the N African Plate: geochemical and isotopic evidence from the tholeiitic and alkaline volcanic rocks of the Hyblean Plateau, Italy. Contributions to Mineralogy and Petrology, 131, 307-322.

Tsuno, K., and Dasgupta, R. (2011) Melting phase relation of nominally anhydrous, carbonated pelitic-eclogite at 2.5–3.0 GPa and deep cycling of sedimentary carbon. Contributions to Mineralogy and Petrology743-763.

Wallace, P.J., and Carmichael, I.S.E. (1994) S-speciation in submarine basaltic glasses as determined by measurements of SK-alpha X-ray wavelength shifts. American Mineralogist, 79, 161-167.

Walter, M.J. (1998) Melting of garnet peridotite and the origin of komatiite and depleted lithosphere. Journal of Petrology, 39, 29-60.

Wasylenki, L.E., Baker, M.B., Kent, A.J.R., and Stolper, E.M. (2003) Near-solidus melting of the shallow upper mantle: Partial melting experiments on depleted peridotite. Journal of Petrology, 44, 1163-1191.

Watson, E.B. (1977) Partitioning of manganese between forsterite and silicate liquid. Geochimica Et Cosmochimica Acta, 41, 1363-1374.

West, H.B., Garcia, M.O., Gerlach, D.C., and Romano, J. (1992) Geochemistry of tholeiites from Lanai, Hawaii. Contributions to Mineralogy and Petrology, 112, 520-542.

Wood, B.J., and Blundy, J.D. (2003) Trace element partitioning under crustal and uppermost mantle conditions: the influences of ionic radius, cation charge, pressure, and temperature. In R.W. Carlson, Ed. The Mantle and Core - Treatise on Geochemistry Vol. 2, p. 395-425. Elsevier.

Wood, B.J., Bryndzia, L.T., and Johnson, K.E. (1990) Mantle oxidation state and its relationship to tectonic environment and fluid speciation. Science, 248, 337-345.

Workman, R.K., and Hart, S.R. (2005) Major and trace element composition of the depleted MORB mantle (DMM). Earth and Planetary Science Letters, 231, 53-72.

Yao, L.J., Sun, C.G., and Liang, Y. (2012) A parameterized model for REE distribution between low-Ca pyroxene and basaltic melts with applications to REE partitioning in low-Ca pyroxene along a mantle adiabat and during pyroxenite-derived melt and peridotite interaction. Contributions to Mineralogy and Petrology, 164, 261-280.

Zhang, Y.X. (2010) Diffusion in Minerals and Melts Theoretical Background. In Y.X. Zhang, and D.J. Cherniak, Eds. Diffusion in Minerals and Melts, 72, p. 5-57. Mineralogical Soc Amer, Chantilly.

Zindler, A., and Hart, S. (1986) Chemical geodynamics. Annual Review of Earth and Planetary Sciences, 14, 493-571.

681 **Table Captions**

682

683 **TABLE 1.** Cu, Ga and Ge concentrations of olivine, orthopyroxene, clinopyroxene, melt and
684 starting materials (in μg/g). Errors are given in μg/g in parentheses and represent one sigma
685 standard deviations with respect to the mean value calculated based on ~3-5 replicate analyses of
686 mineral and melt phases. Cu, Fe, Ga, and Ge loss or gain are reported in % change (gain is
687 positive, loss is negative) in experiments where all identified phases have been analyzed.
688 Calculations are based on estimates of modal proportions by mass balance between trace element
689 concentrations in bulk starting materials, minerals and quenched melts. *, ** and *** indicates
690 that Mix 1, Mix 2 and Mix 3 have been used for the experiment, respectively.

691

692 **TABLE 2.** Average partition coefficients of Cu, Ga, and Ge between olivine, orthopyroxene,
693 clinopyroxene, and melt from this study. Errors in parentheses are on the last digit(s), and
694 correspond to propagated errors. *, ** and *** indicates that Mix 1, Mix 2 and Mix 3 have been
695 used for the experiment, respectively. [#] Different from recommended value.

696

697 **TABLE 3.** [a] Liu et al. (2014), [b] Davis et al. (2013), [c] McDade et al. (2003), [d] Mallmann and
698 O'Neill (2009), [e] Pertermann et al. (2004), [f] Le Roux et al. (2011), [g] Righter et al. (2006), [h] Lee
699 et al. (2012), [i] Fellows and Canil (2012), [j] Yao et al. (2012), [k] Canil and Fedortchouk (2000), [l]
700 Canil and Fedortchouk (2001). $D_{Cu}^{Sp/melt}$ from Liu et al. (2014) is only available from
701 experiments performed in oxidizing conditions. $D_{V}^{Mineral/melt}$ and $D_{Sc}^{Mineral/melt}$ values from
702 Mallmann and O'Neill (2009) were taken from experiments performed at 1 atm and QFM ~ 0.
703 Values without annotations indicate that partition coefficients are from this study. Errors for our

704 study correspond to standard deviations of averages in Table 2. If no error is reported, the
705 recommended value has been calculated. For example, $D_{Ga}^{Px/melt}$ at 3 GPa has been calculated
706 from our parametrization with an Al_2O_3 content of pyroxene of 6.5 wt.% (based on the
707 parametrization of Hirschman et al. 2009). Errors for other studies are reported, when available,
708 on the last digit(s) and represent the standard deviations of averages of all referenced studies.
709 $D_{Cu\ lower\ range}$ line provides minimum values for Cu partition coefficients. Values *in italics*
710 indicate that *D*s are estimated from mineral compositions appropriate for other lithologies and
711 therefore may not be as accurate as other values (e.g., $D_{Ge}^{Cpx/melt}$ in MORB-like eclogite is taken
712 from $D_{Ge}^{Cpx/melt}$ in garnet peridotite).
713

Figure Captions

FIGURE 1. Cu (a), Ga (b) and Ge (c) concentrations (in μg/g) obtained by EPMA and LA-ICP-MS in six quenched glasses and one clinopyroxene. Quenched glasses are from experiments G81, G84, G92, G94, G99, and G100, and clinopyroxene is from experiment G110. Error bars correspond to the one sigma standard deviation based on replicate concentration measurements. When the error bar is not visible, the symbol is larger than the standard deviation.

FIGURE 2. Cu partition coefficients between olivine, orthopyroxene, clinopyroxene and melt derived from this study plotted against Cu in % change. Negative values indicate Cu loss, positive values indicate Cu gain. Error bars correspond to the standard deviation of averaged partition coefficients. Error bars correspond to the one sigma standard deviation of averaged partition coefficients.

FIGURE 3. Cu partition coefficients between clinopyroxene and melt versus (a) Cu concentrations in clinopyroxene (in μg/g) and (b) Na_2O content in clinopyroxene (in wt. %). Horizontal and vertical error bars correspond to the one sigma standard deviation based on replicate measurements and the one sigma standard deviation of averaged partition coefficients from this study, respectively. The dashed line in (a) illustrates how the increase in Cu partition coefficients may be partly due to a non-henrian behavior. The two dashed lines in (b) illustrate how the increase in Cu partition coefficients is also strongly correlated with the Na_2O content of Cpx. Variations in (a) and (b) are also controlled by variations in starting materials and *P-T* conditions.

737

738 **FIGURE 4.** Ga partition coefficients between (a) clinopyroxene and melt versus Al_2O_3 content
739 (in wt. %) in clinopyroxene and (b) between orthopyroxene and melt versus Al_2O_3 content (in
740 wt. %) in orthopyroxene. Vertical error bars correspond to the one sigma standard deviation with
741 respect to the mean partition coefficients derived from this study. The equations are obtained by
742 fitting data from this study and previous experimental data (Malvin and Drake 1987; Hart and
743 Dunn 1993; Mallmann and O' Neill 2009; Davis et al. 2013). The dashed lines correspond to
744 representative pyroxene compositions calculated from Hirschmann et al. (2009) for low-*P* spinel
745 peridotite (1.5 GPa), intermediate-P spinel peridotite (2.8 GPa), high-*P* garnet peridotite (3 GPa),
746 and high-*P* garnet peridotite (4 GPa), and representative pyroxene compositions taken from
747 Pertermann and Hirschmann et al. (2003a) in MORB-like eclogite (2-3 GPa).

748

749 **FIGURE 5.** Ge partition coefficients between orthopyroxene and melt versus temperature
750 compared to data from Davis et al. (2013). The equation is obtained by fitting data from this
751 study and previous experimental data.

752

753 **FIGURE 6.** Cu (a), Ga (b) and Ge (c) partition coefficients between olivine, orthopyroxene,
754 clinopyroxene and melt derived from this study and partition coefficients from the literature. + Malvin and Drake, 1987 (1 atm / 1300 °C / MORB-like melt); ✳ Hart and Dunn 1993 (3 GPa /
755 1380 °C / alkali basalt); ⊞ Gaetani and Grove 1997 (1 atm / 1350 °C / silicate melt with 51-56
756 wt. % SiO_2); ○ Mallmann and O' Neill, 2009 (1 atm-3 GPa / 1300-1450 °C / MORB-like melt);
757 △ Fellows and Canil, 2012 (1 GPa / 1250-1525 °C / basaltic melt); □ Lee et al., 2012 (natural
758 phenocryst-groundmass pairs); ▣ Yao et al. 2012 (2 GPa / 1380-1425 °C / basaltic andesite); ▲
759

760 Davis et al. 2013 (3GPa / 1460-1475 °C / MORB-like melt); ◇ Liu et al., 2014 (all data. 1-3
761 GPa/ 1150-1300 °C/ hydrous silicate melt); ◈ Liu et al. 2014 (subset. 'MORB' starting material
762 only, Cpx have higher Na_2O content); ◆ Liu et al. 2014 (subset. 'oxidized' experiments only, >
763 QFM + 3). Error bars are only reported for this study and correspond to the one sigma standard
764 deviation with respect to the mean partition coefficients.
765
766
767 **FIGURE 7.** Cu concentrations (in μg/g) in (a) orthopyroxene and olivine, and (b) in
768 clinopyroxene and olivine from this study, compared with experimental (Fellows and Canil
769 2012; Liu et al. 2014) and natural (Lee et al. 2012) data. Only data obtained in reducing
770 conditions in Liu et al. (2014), and with concentrations lower than 100 ppm, are presented. Data
771 from Fellows and Canil (2012) are only presented for comparison and not included in the
772 regression, as the data were reported to be below detection limit. The range of natural data is
773 detailed in the insets. Trendlines are forced to go through the origin and slopes correspond to
774 intermineral partition coefficients. Trendlines in the insets are the same as in the main figure to
775 show the fit with natural data. Error bars correspond to the one sigma standard deviation based
776 on replicate concentration measurements. If no error bar is reported, error is smaller than the
777 symbol.
778
779 **FIGURE 8.** (a) Cu content of peridotite-derived aggregate melts (in μg/g) produced by near
780 fractional melting of a sulfide-free source, calculated using partition coefficients from this study
781 ($D^{peridotite/melt} \sim 0.12$), and Lee et al. (2012) and Liu et al. (2014) studies ($D^{peridotite/melt} \sim$
782 0.05). We assume that the source contains 30 μg/g Cu (Sun 1982; Salters and Stracke 2004) and

~ 200 µg/g S (Chaussidon et al. 1989; Lorand 1991; O'Neill 1991; Lee et al. 2012; Nielsen et al. 2014). Mean *F* is the melt fraction. The MORB field is from Lee et al. (2012) (b) Same parameters as (a), assuming a source that contains 0.06 wt. % sulfides. $D^{peridotite/melt}$ ranges from 0.49 (Lee et al. 2012) to 0.60 (this study).

FIGURE 9. (a) Ga concentration (in µg/g) versus TiO_2 (wt. %) in melts with > 8 wt. % MgO from various tectonic environments. MORB data are from Jenner and O'Neill (2012), other data have been compiled from georoc (http://georoc.mpch-mainz.gwdg.de/georoc/) and include a number of previously published studies (West et al. 1992; Trua et al. 1998; Barrie et al. 1999; Briand et al. 2002; Ntaflos and Richter 2003; Hartlaub et al. 2004; Greene et al. 2009; Ma et al. 2011).

Partial melting trends have been calculated using recommended *D*s from this study and from the literature (Table 3). Melting degrees are reported next to melting trends.

FIGURE 10. FRTE, Ga, and Ge partition coefficients between (a) olivine and melt, (b) orthopyroxene and melt, and (c) clinopyroxene and melt in spinel peridotite, garnet peridotite and MORB-like eclogite. (d) FRTE, Ga, and Ge bulk partition coefficients between spinel peridotite, garnet peridotite, MORB-like eclogite and melt. All partitioning data and uncertainties are from Table 3. Bulk *D*s were calculated using the same modal compositions as in melting models (see text). If no error bar is visible, uncertainty reported in Table 3 is smaller than the symbol.

806

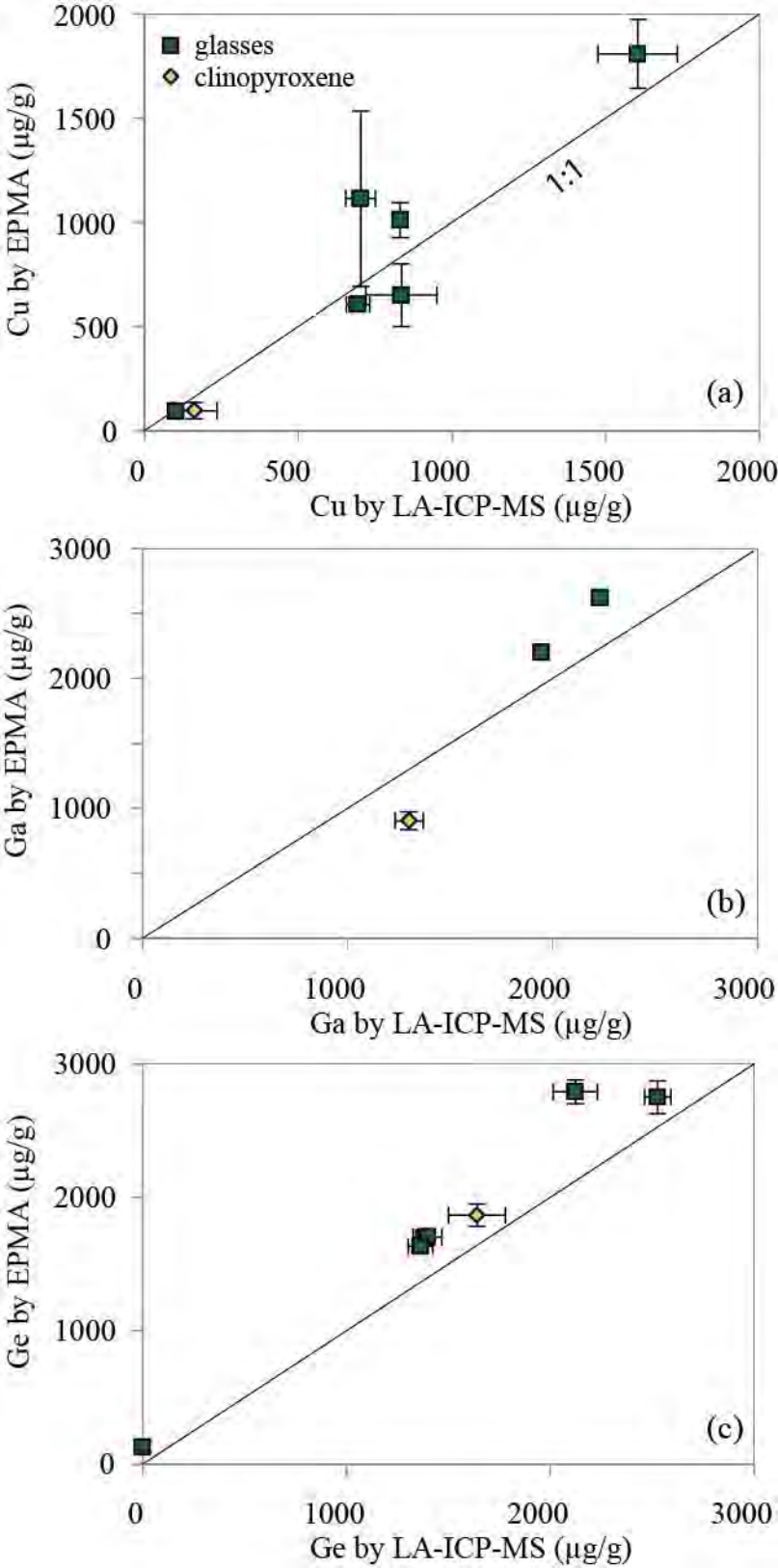
glasses
clinopyroxene
1:1
(a)
Cu by EPMA (µg/g)
Cu by LA-ICP-MS (µg/g)
0
500
1000
1500
2000
(b)
Ga by EPMA (µg/g)
Ga by LA-ICP-MS (µg/g)
0
1000
2000
3000
(c)
Ge by EPMA (µg/g)
Ge by LA-ICP-MS (µg/g)

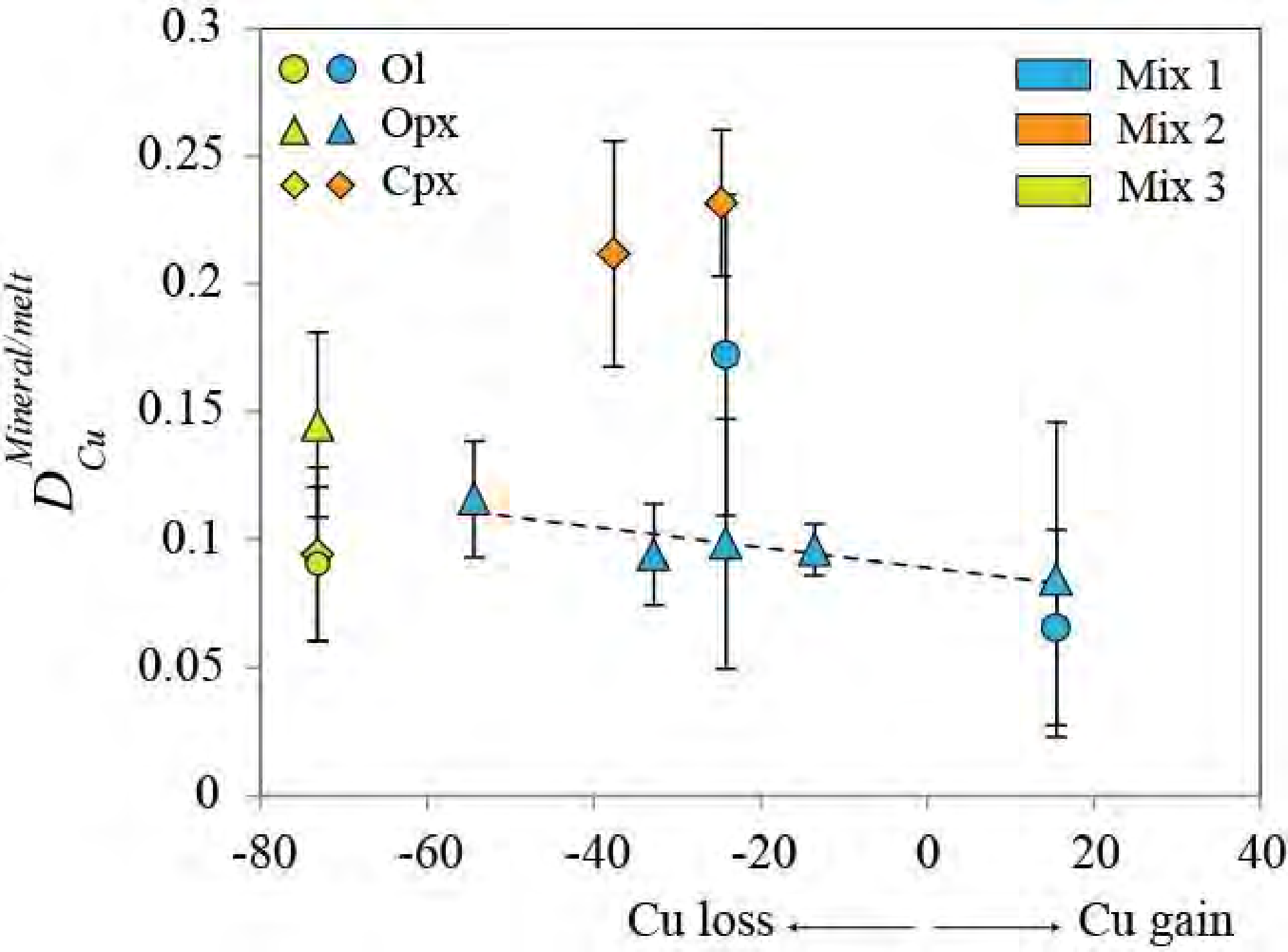
0.3
0.25
0.2
0.15
0.1
0.05
0
$D_{Cu}^{Mineral/melt}$
Ol
Opx
Cpx
Mix 1
Mix 2
Mix 3
-80
-60
-40
-20
0
20
40
Cu loss
Cu gain

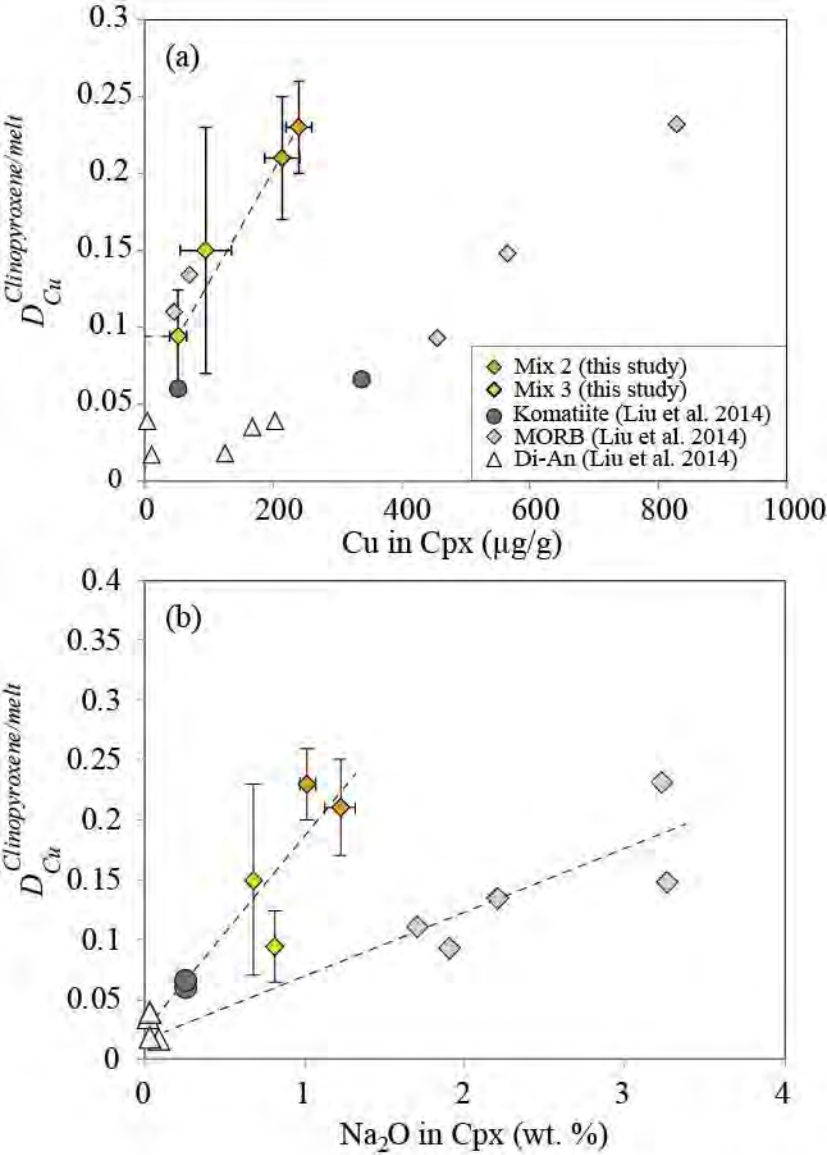
(a)
$D_{Cu}^{Clinopyroxene/melt}$
Cu in Cpx (μg/g)
Mix 2 (this study)
Mix 3 (this study)
Komatiite (Liu et al. 2014)
MORB (Liu et al. 2014)
Di-An (Liu et al. 2014)
(b)
$D_{Cu}^{Clinopyroxene/melt}$
Na_2O in Cpx (wt. %)

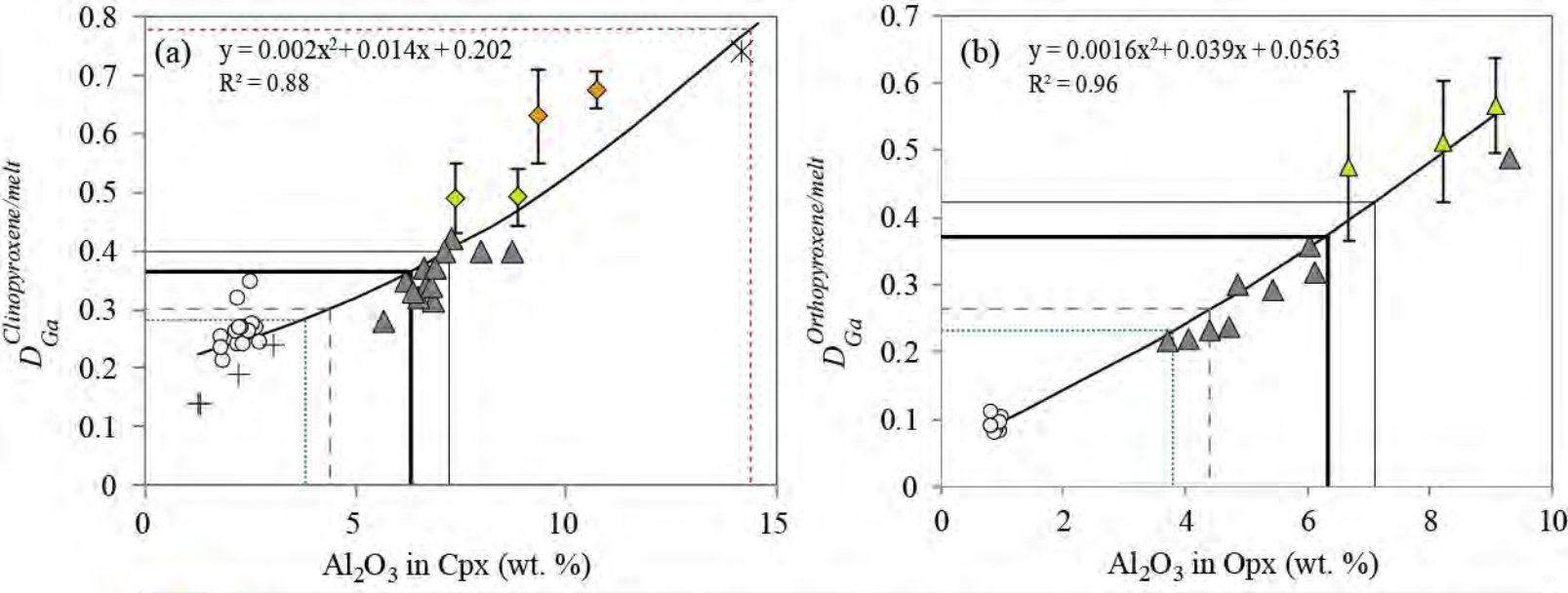
(a)
y = 0.002x²+ 0.014x + 0.202
R² = 0.88
$D_{Ga}^{Clinopyroxene/melt}$
Al_2O_3 in Cpx (wt. %)
(b)
y = 0.0016x²+ 0.039x + 0.0563
R² = 0.96
$D_{Ga}^{Orthopyroxene/melt}$
Al_2O_3 in Opx (wt. %)
Mix 2 (this study)
Mix 3 (this study)
Malvin and Drake (1987)
Hart and Dunn (1993)
Mallmann and O'Neill (2009)
Davis et al. (2013)
1.5 GPa spinel peridotite
2.8 GPa spinel peridotite
3 GPa garnet peridotite
4 GPa garnet peridotite
MORB-like
eclogite pyroxene (2-3 GPa)

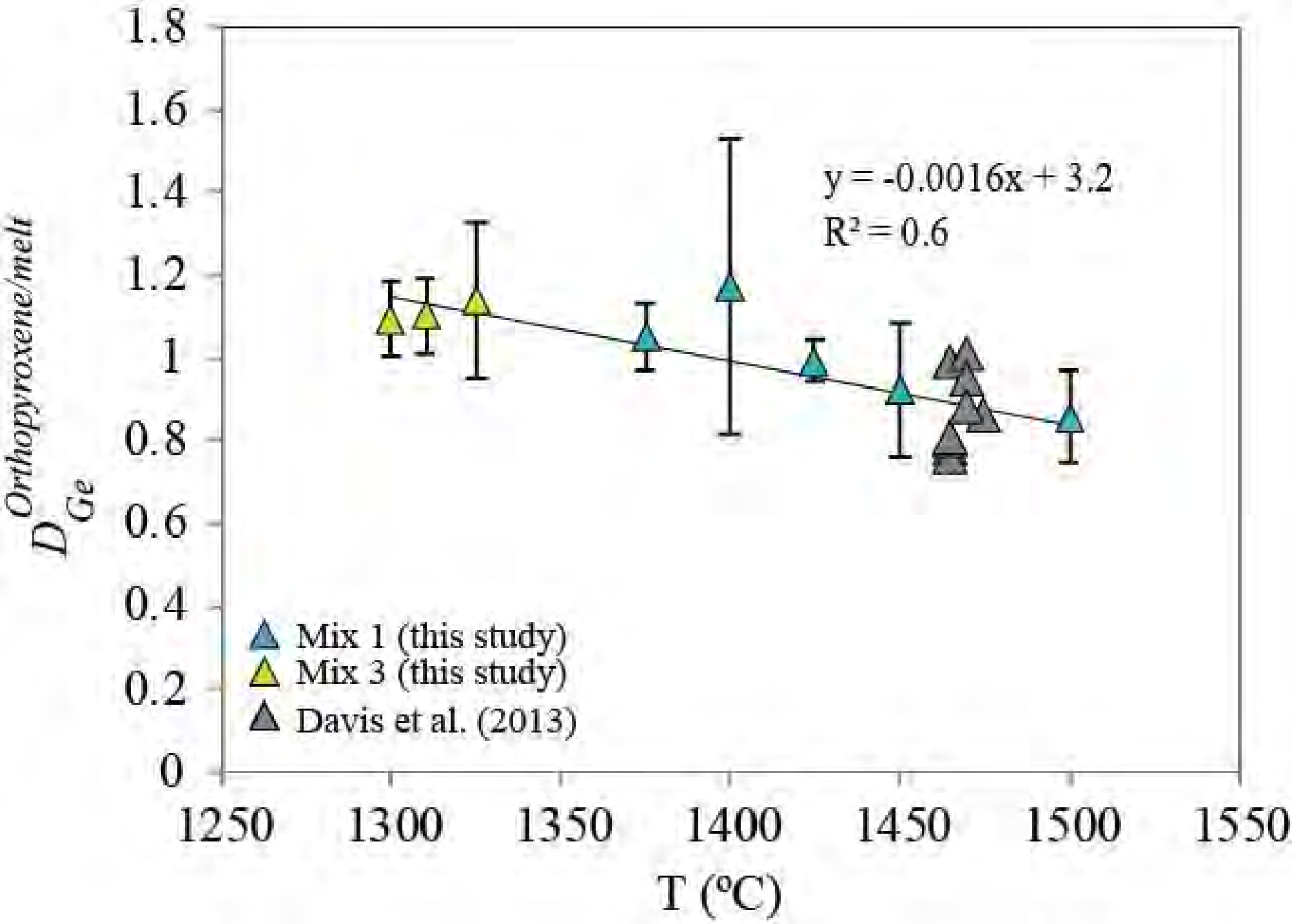
1.8
1.6
1.4
1.2
1
0.8
0.6
0.4
0.2
0
$D_{Ge}^{Orthopyroxene/melt}$
y = -0.0016x + 3.2
R² = 0.6
Mix 1 (this study)
Mix 3 (this study)
Davis et al. (2013)
1250
1300
1350
1400
1450
1500
1550
T (°C)

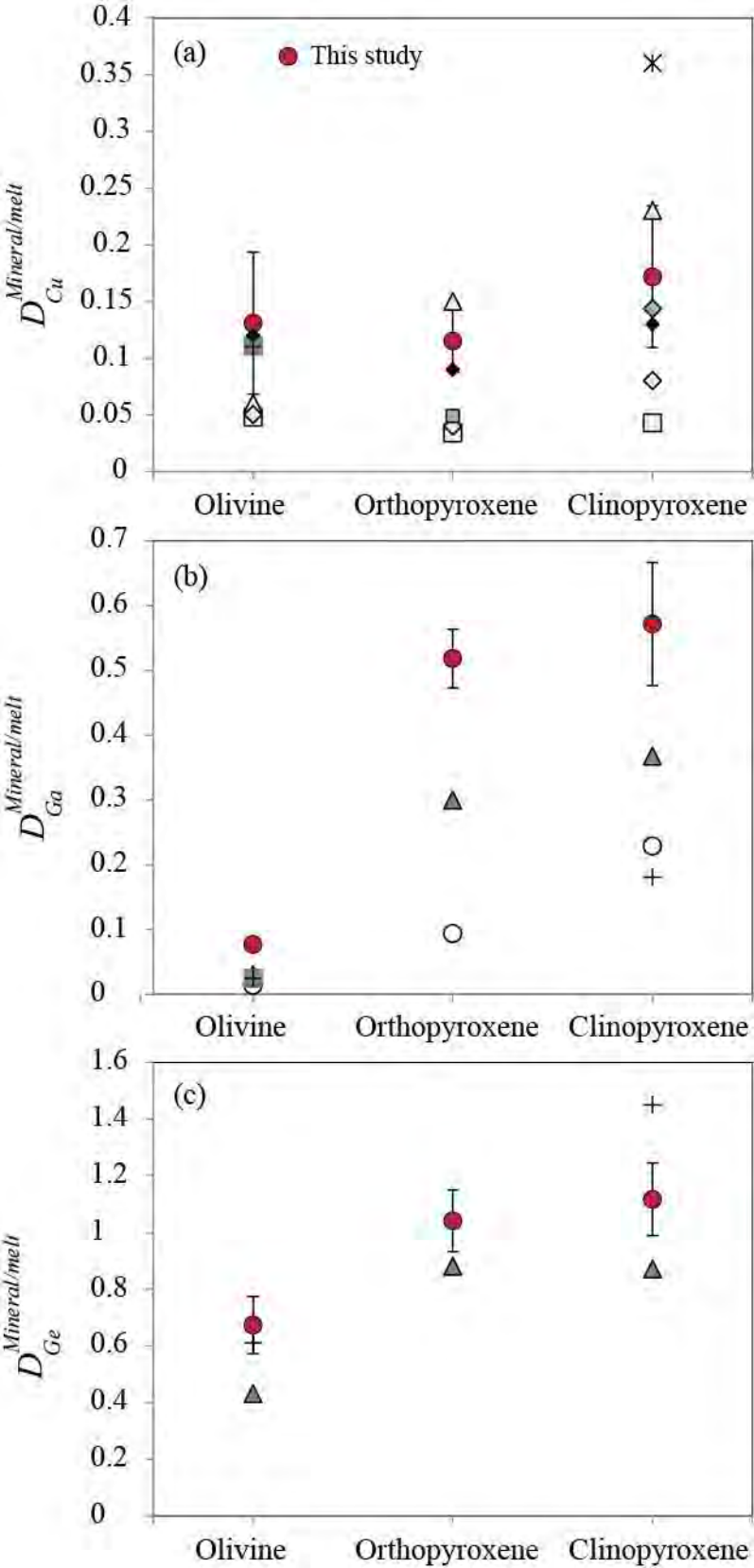
(a)
This study
$D_{Cu}^{Mineral/melt}$
0.4
0.35
0.3
0.25
0.2
0.15
0.1
0.05
0
Olivine
Orthopyroxene
Clinopyroxene
(b)
$D_{Ga}^{Mineral/melt}$
0.7
0.6
0.5
0.4
0.3
0.2
0.1
0
Olivine
Orthopyroxene
Clinopyroxene
(c)
$D_{Ge}^{Mineral/melt}$
1.6
1.4
1.2
1
0.8
0.6
0.4
0.2
0
Olivine
Orthopyroxene
Clinopyroxene

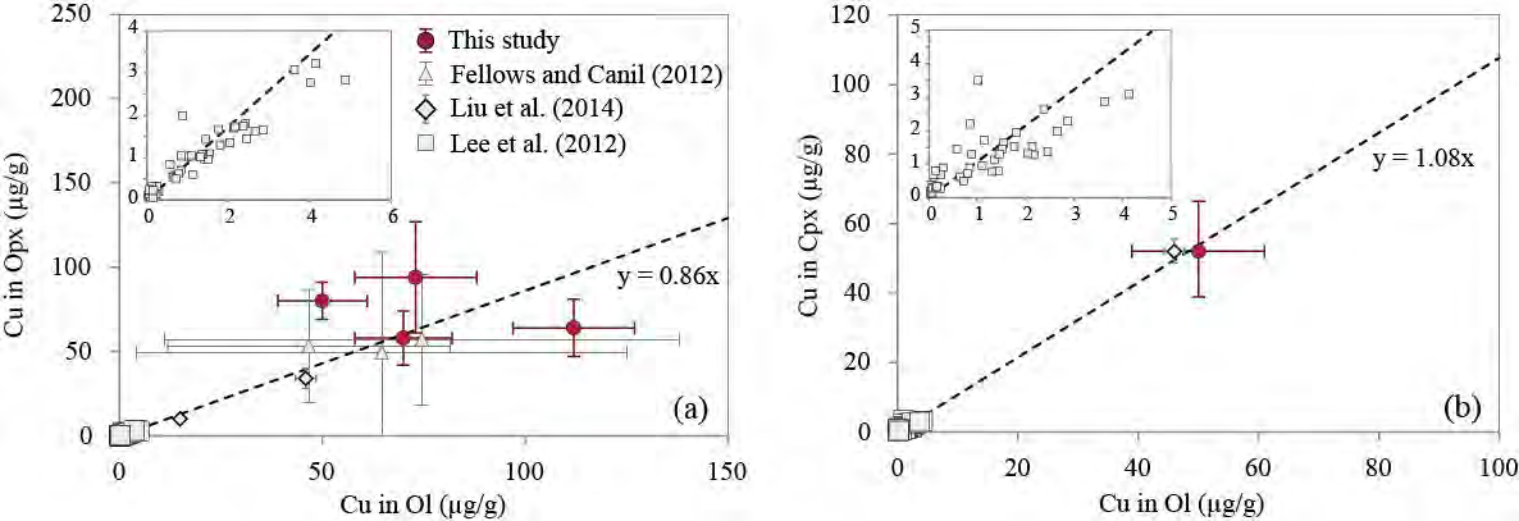
This study
Fellows and Canil (2012)
Liu et al. (2014)
Lee et al. (2012)
y = 0.86x
(a)
Cu in Opx (µg/g)
Cu in Ol (µg/g)
y = 1.08x
(b)
Cu in Cpx (µg/g)
Cu in Ol (µg/g)

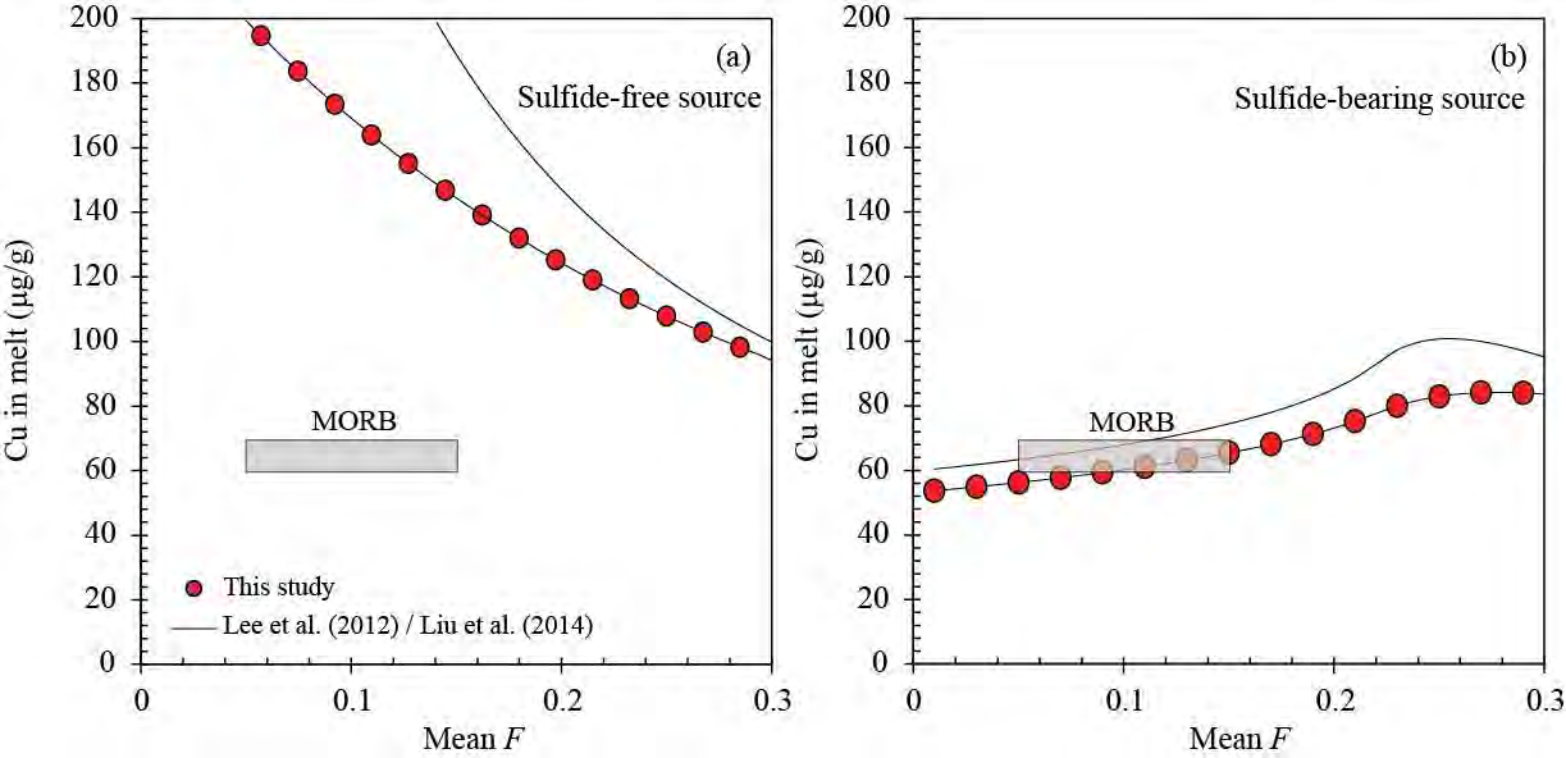
(a)
Sulfide-free source
(b)
Sulfide-bearing source
Cu in melt (µg/g)
Mean F
MORB
This study
Lee et al. (2012) / Liu et al. (2014)
0
20
40
60
80
100
120
140
160
180
200
0.1
0.2
0.3

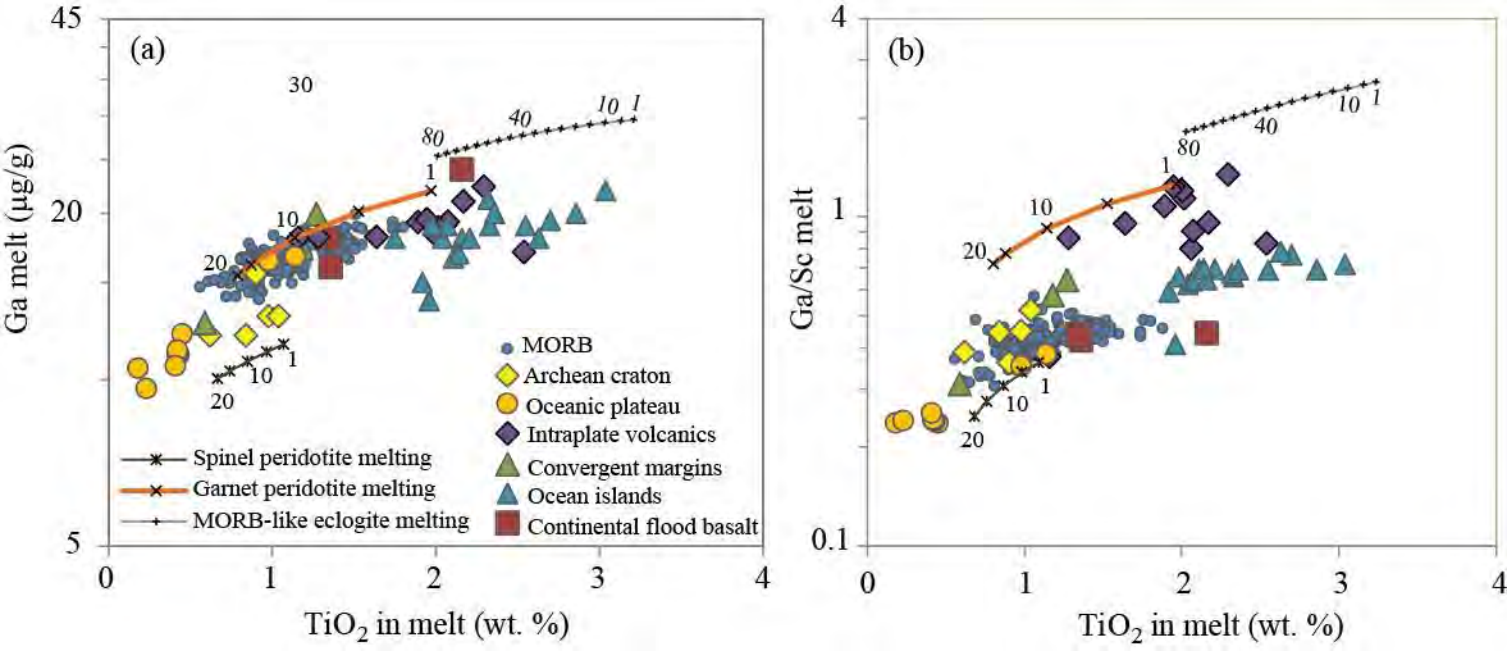
(a)
(b)
Ga melt (μg/g)
Ga/Sc melt
TiO2 in melt (wt. %)
TiO2 in melt (wt. %)
MORB
Archean craton
Oceanic plateau
Intraplate volcanics
Convergent margins
Ocean islands
Continental flood basalt
Spinel peridotite melting
Garnet peridotite melting
MORB-like eclogite melting

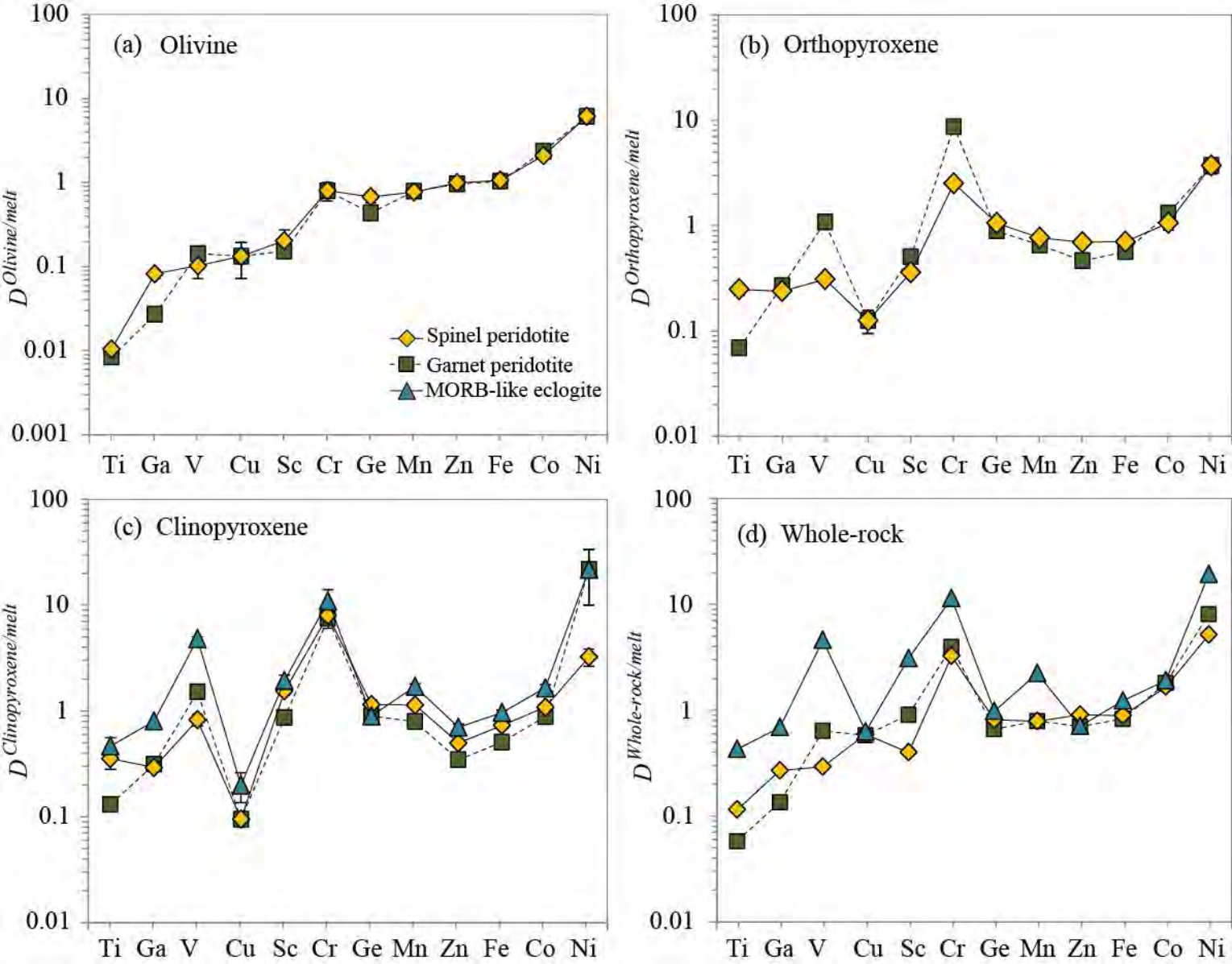
(a) Olivine
(b) Orthopyroxene
(c) Clinopyroxene
(d) Whole-rock
D Olivine/melt
D Orthopyroxene/melt
D Clinopyroxene/melt
D Whole-rock/melt
100
10
1
0.1
0.01
0.001
Ti Ga V Cu Sc Cr Ge Mn Zn Fe Co Ni
Spinel peridotite
Garnet peridotite
MORB-like eclogite

TABLE 1. Cu, Ga, and Ge concentrations in mantle minerals and melt (in µg/g) and elemental losses (in % change)

	Olivine			Orthopyroxene			Clinopyroxene		
	Cu	Ga	Ge	Cu	Ga	Ge	Cu	Ga	Ge
G81*	73 (15)	-	1060 (44)	94 (33)	-	1566 (219)	-	-	-
G83*	-	-	-	55 (7)	-	1850 (462)	-	-	-
G84*	112 (15)	-	958 (52)	64 (17)	-	1460 (138)	-	-	-
G90*	-	-	-	85 (6)	-	1675 (70)	-	-	-
G92*	-	-	-	57 (11)	-	1617 (40)	-	-	-
G93**	-	-	-	-	-	-	240 (20)	1556 (129)	3804 (169)
G94**	-	-	-	-	-	-	214 (27)	1768 (37)	3056 (193)
G107***	50 (11)	136 (21)	1202 (95)	80 (11)	846 (126)	1912 (284)	52 (13)	810 (79)	1644 (166)
G109***	70 (12)	113 (59)	1280 (105)	58 (16)	754 (163)	1766 (88)	-	-	-
G110***	-	-	-	80 (8)	1042 (103)	1858 (90)	95 (40)	904 (68)	1866 (84)

	Melt						
	Cu	Ga	Ge	Cu % change	Fe % change	Ga % change	Ge % change
G81*	1113 (421)	-	1697 (60)	15.5	3.7	-	18.7
G83*	475 (33)	-	1578 (95)	-54.4	7.1	-	23.9
G84*	650 (150)	-	1702 (57)	-24.2	-1.8	-	17.2
G90*	885 (31)	-	1592 (54)	-13.5	-1.7	-	18.1
G92*	605 (10)	-	1630 (47)	-32.8	-1.1	-	17.8
G93**	1036 (42)	2470 (115)	2954 (112)	-24.7	1.0	1.8	15.2
G94**	1010 (83)	2620 (74)	2790 (89)	-37.6	-4.4	3.6	5.3
G107***	552 (62)	1652 (54)	1682 (24)	-73.2	6.5	-6.2	-0.6
G109***	358 (48)	1583 (26)	1617 (55)	-	-	-	-
G110***	634 (80)	1840 (33)	1686 (63)	-	-	-	-

TABLE 2. Partition coefficients of Cu, Ga, and Ge between mantle minerals and melt

			D_{Cu}			D_{Ga}			D_{Ge}		
	P (Gpa)	*T (°C)*	Ol/melt	Opx/melt	Cpx/melt	Ol/melt	Opx/melt	Cpx/melt	Ol/melt	Opx/melt	Cpx/melt
G109***	1.5	1300	0.20 (6)	0.16 (7)	-	0.07 (4)	0.48 (11)	-	0.79 (9)	1.09 (9)	-
G110***	1.5	1310	-	0.13 (3)	0.15 (8)	-	0.57 (7)	0.49 (5)	-	1.10 (9)	1.11 (9)
G107***	1.5	1325	0.09 (3)	0.14 (4)	0.09 (3)	0.08 (2)	0.51 (9)	0.49 (6)	0.71 (7)	1.14 (19)	0.98 (11)
G90*	1.5	1375	-	0.10 (1)	-	-	-	-	-	1.05 (8)	-
G94**	2	1290	-	-	0.21 (4)	-	-	0.67 (3)	-	-	1.10 (10)
G93**	2	1320	-	-	0.23 (3)	-	-	0.63 (8)	-	-	1.29 (11)
G83*	2	1400	-	0.12 (2)	-	-	-	-	-	1.17 (36)	-
G92*	2	1425	-	0.09 (2)	-	-	-	-	-	0.99 (5)	-
G81*	2	1450	0.07 (4)	0.08 (6)	-	-	-	-	0.62 (5)	0.92 (16)	-
G84*	2	1500	0.17 (6)	0.10 (5)	-	-	-	-	0.56 (5)	0.86 (11)	-
average			0.13 (6)	0.12 (3)	0.17 (6)[#]	0.08 (1)	0.52 (5)[#]	0.57 (10)[#]	0.67 (10)	1.04 (11)	1.12 (13)

TABLE 3.FRTE, Ga, and Ge partition coefficients suitable to model mantle melting at QFM < 1.5

	Low-*P* (<2 GPa) spinel peridotite melting				High-*P* (3GPa) garnet peridotite melting				MORB-like eclogite melting (2-3 GPa)	
	Ol/melt	Opx/melt	Cpx/melt	Sp/melt	Ol/melt	Opx/melt	Cpx/melt	Gt/melt	Cpx/melt	Gt/melt
D_{Cu}	0.13 (6)	0.12 (3)	0.09	0.25 (8)[a]	*0.13 (6)*	*0.12 (3)*	*0.09*	0.042 (6)[a]	0.19 (6)[a]	0.042 (6)[a]
D_{Ga}	0.08 (1)	0.23	0.28	6.50 (5)[b]	0.026 (1)[b]	0.38	0.37	0.390 (7) [b]	0.78	*0.39(7)* [b]
D_{Ge}	0.67 (10)	1.04 (11)	1.12 (13)	0.40 (4)[b]	0.43 (1)[b]	0.87 (2)[b]	0.87 (3)[b]	1.51 (3)[b]	*0.87 (3)* [b]	*1.51(3)* [b]
$D_{Cu\ lower\ range}$	0.06 (1)[a,h,i]	0.04 (1)[a,h,j]	0.06 (3)[a,h]							
D_{Ti}	0.01[c]	0.24 (3)[c]	0.34 (7)[c]	0.084 (8)[b]	0.0080 (7)[b]	0.0656 (18)[b]	0.124 (6)[b]	0.262 (4)[b]	0.45 (9)[e]	0.39 (11)[e]
D_{Sc}	0.20 (7)[d]	0.35 (2)[d]	1.51 (13)[d]	0.058 (8)[b]	0.150 (3)[b]	0.495 (11)[b]	0.84 (4)[b]	5.98 (11)[b]	1.90 (24)[e]	8 (2)[e]
D_{V}	0.10 (3)[d,l]	0.30[d]	0.8 (1)[d,k]	2.75 (19)[b]	0.140 (3)[b]	1.06 (3)[b]	1.48 (4)[b]	1.84 (4)[b]	4.77 (23)[e]	4 (2)[e]
D_{Cr}	0.8 (2)[d]	2.5[d]	8 (2)[d]	54 (11)[b]	0.79 (6)[b]	8.8 (5)[b]	7.5 (6)[b]	10.2 (4)[b]	11 (3)[e]	13 (9)[e]
D_{Mn}	0.77 (2)[f]	0.75 (8)[f]	1.11 (5)[f]	0.46 (3)[b]	0.781 (14)[b]	0.640 (12)[b]	0.768 (18)[b]	1.241 (17)[b]	1.67 (11)[e]	4.6 (5)[e]
D_{Zn}	0.99 (14)[f]	0.68 (7)[f]	0.48[f]	5.2 (5)[b]	0.96 (4)[b]	0.451 (17)[b]	0.333 (17)[b]	0.213 (9)[b]	0.68 (5)[e]	0.89 (11)[e]
D_{Fe}	1.06 (5)[f]	0.69 (5)[f]	0.71 (4)[f]	0.95 (6)[b]	1.034 (16)[b]	0.55 (1)[b]	0.49 (1)[b]	0.654 (7)[b]	0.94 (5)[e]	2.5 (3)[e]
D_{Co}	2.1 (2)[f]	1.04 (15)[f]	1.06 (9)[f]	3.0 (6)[b]	2.37 (9)[b]	1.29 (14)[b]	0.86 (4)[b]	0.83 (2)[b]	1.62 (12)[e]	3.18 (36)[e]
D_{Ni}	6.2 (7)[f]	3.7 (6)[f]	3.2 (6)[f]	10[g]	*6.2 (7)* [f]	*3.7 (6)* [f]	*22 (12)* [e]	*8 (7)* [e]	22 (12)[e]	8 (7)[e]